ANNALS OF GEOPHYSICS, 68, 4, V453, 2025; doi:10.4401/ag-9253
OPEN ACCESS

A multidisciplinary strategy based on geophysical and geochemical data to investigate hydrothermal circulation along the rift zones of Mt. Etna volcano (Italy)

Salvatore Giammanco*[,1], Samuel Maucourant[1], Rosalba Napoli[1], Filippo Greco[1], Antonino Sicali[1]

(1) Istituto Nazionale di Geofisica e Vulcanologia, Osservatorio Etneo – Sezione di Catania, Catania, Italy

Article history: received January 17, 2025; accepted September 10, 2025

Abstract

We surveyed the South Rift and Northeast Rift of Mt. Etna volcano in order to assess the presence and the spatial extent of shallow hydrothermal activity linked with magma degassing along the main feeder systems of the volcano. Surveys were carried out across the two rift zones at altitude between 1500 and 2500 m a.s.l. Soil CO_2 effluxes, soil heat fluxes, self-potential intensity, simultaneously with magnetic surveys, were measured for the first time together in 2017, both along profiles of measurement points and over networks of points. Several convective hydrothermal cells were found close together, particularly on the South Rift where they occupied a large portion of this rift. This suggested the existence of a complex plexus of volcano-tectonic structures, highly permeable to volcanic fluids, that are all potential pathways for new magma intrusions, as they appear well connected with the portions of the central feeder conduits that allow for efficient magma degassing. Gravity measurements acquired successively along the South Rift strongly support this hypothesis. The Northeast Rift showed only one major hydrothermal convective cell, centered along the 2002 eruptive fissure, and a minor one a few hundred meters west of it. These surveys were repeated in 2018, although only partially. The 2018 measurements showed a strong decrease in the overall intensity of hydrothermal circulation along the Northeast Rift area and in most of the South Rift areas surveyed in 2017. This was explained as indication of strong migration of high-enthalpy fluids from the two rift zones following magma transfer along the main conduits of the volcano towards its summit. Similar conclusions were drawn from the observed variations in gravity data from 2020 to 2021. The hypothesized magma transfer episodes seem to be coherent with the subsequent occurrence of the December 2018 flank eruption and of the 2020-2021 sequence of paroxysmal summit eruptions.

Keywords: Mt. Etna; Hydrothermal systems; Rift zones; Volcano monitoring; Multidisciplinary approach

1. Introduction

The dynamics of an active volcano are complex and often difficult to study and monitor, thus underscoring the need for innovative strategies in volcanology, potentially based on multidisciplinary approaches. Given that volcanoes are primarily thermodynamic engines that release the excess heat produced inside the Earth to outer space through magmatic processes, including magmatic degassing during non-eruptive periods, there has been a particular focus on studying the release of heat from volcanoes, both directly and indirectly. Direct methods include measuring the heat flux from active magmatic emissions during eruptions or during long-standing Strombolian or lava lake activity using remote sensing techniques (Oppenheimer and Francis, 1997; Harris et al., 1999; Mouginis-Mark et al., 2000; Spampinato et al., 2011). However, this is not always straightforward and is often unfeasible. The indirect methods primarily entail surveying the release of gas and heat from hydrothermal systems to estimate the total heat flux exchanged by magmatic fluids with shallow groundwater and the atmosphere. This is an equally challenging endeavor, but often more feasible due to more straightforward logistics for fieldwork and greater safety of the study areas.

Indeed, the interaction between high-enthalpy fluids released from magma and shallow aquifers may result in the formation of hydrothermal systems, both in active and dormant volcanoes. However, in some cases, these systems are absent or underdeveloped outside the main active craters. For instance, Hekla in Iceland and Nyiragongo in Congo are examples of volcanoes where such systems are either absent or not developed outside the main crater(s). The evolution of these systems is contingent upon the quantity of mass and heat transported by new magma intruding at shallow levels into the crust, as well as the volume and composition of fluids released during magma ascent. Consequently, monitoring these systems over time may offer valuable insights into the potential future activity of a volcano. In particular, large hydrothermal cells tend to form and develop predominantly along rift zones on basaltic volcanoes. These are structurally weak volcano-tectonic lines that typically originate at the summit of a volcano and extend downslope along its flanks. Magma intrudes and erupts at the surface with greater frequency along rift zones than in non-rift areas. This is due to the higher crustal permeability observed in these zones, which is a consequence of the persistent volcano-tectonic stress applied in these regions (Acocella and Neri, 2003).

Mt. Etna volcano is an illustrative example of these rules. Mount Etna is one of the most active volcanoes in the world and is also a large mountain, covering a total surface of approximately 1,200 km^2 with its top reaching 3403 m above sea level (a.s.l.). Currently, Mt. Etna erupts alkali basalts, which range in composition from hawaiites to trachybasalts, and constitute the majority of the volcanic pile (Chester et al., 1985; Tanguy et al., 1997). In the last decades, Etna's eruptions have been primarily characterized by violent and short-lived summit eruptions with lava fountains and large emission of volcanic ash in the atmosphere (Branca and Del Carlo, 2005). Both summit eruptions and flank eruptions (i.e., with fissures opening on the volcano's flanks) are also characterized by the emission of lava flows. In some instances, during flank eruptions lava flows have overrun cultivated and/or inhabited areas. However, throughout its 500,000-year lifespan, Mt. Etna has also been responsible for more violent and destructive eruptions, some of which have been classified as Plinian or Sub-Plinian (Branca and Del Carlo, 2005; Branca et al., 2011). Three principal rift zones have been identified on this volcano: the North-East Rift (NER), the South Rift (SR), and the West Rift (WR) (Rittmann, 1973; Kieffer, 1975, 1983; Lo Giudice et al., 1982; Garduño et al., 1997; Acocella and Neri, 2003; Behncke and Neri, 2003a, b) (Fig. 1). The volcanic role of rift zones on Mt. Etna differs from that observed in other basaltic volcanoes, such as the hotspot volcanoes of the Hawaiian archipelago. Unlike these other volcanoes, Etna rifts do not allow for the long-term storage of magma during non-eruptive periods, nor for the formation of shallow magma chambers. In any case, both the South Rift and the North-East Rift were identified as sites of significant and apparently stable hydrothermal circulation. Previous geophysical and geochemical studies conducted along and across the rifts have revealed evidence of hydrothermal circulation, with variable extension and mass/heat release. The extent and intensity of this circulation appear to be contingent upon the methodology employed and the surface characteristics present (Aubert et al., 1984; Aubert and Baubron, 1988; Baubron, 1996; Giammanco et al., 1998; Aubert, 1999; Giammanco and Pecoraino, 2002; Alparone et al., 2004; Maucourant et al., 2014). In some instances, hydrothermal fluids reached the surface, resulting in the emission of visible steam. This phenomenon was observed to occur with considerable steam output rates (Ponte, 1927; Aubert, 1999). Nevertheless, in all cases, both the spatial extent of the surveys and the number of methods employed were constrained.

In recent years, some of the most intense emissions of natural thermal fluids on Mt. Etna have been the subject of study using a multidisciplinary approach based on geophysical parameters (self-potential, gravity, magnetism, heat flux) and geochemical parameters (soil CO_2 efflux) (Maucourant et al., 2014; Napoli et al., 2020). However, once again, surveys were conducted over limited areas, primarily in or around concentrated vents emitting steam and

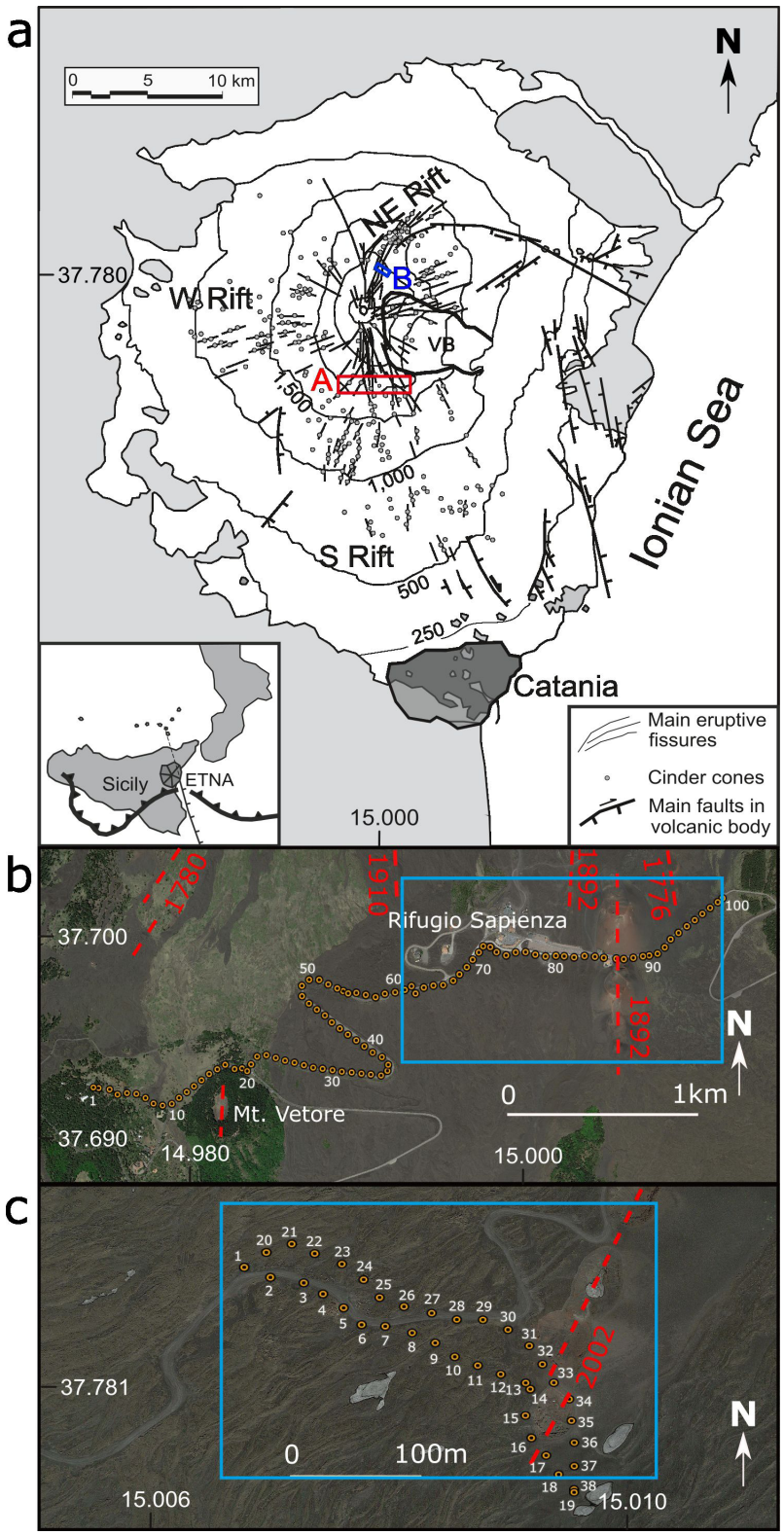

Figure 1. (a) Simplified tectonic map of Mt. Etna, showing the three main rift zones of the volcano (modified from Acocella and Neri, 2003). Inboxes show the study areas (red inbox A = South Rift area; blue inbox B = North-East Rift area); (b) Detailed map of the South Rift study area, with location of sampling sites (yellow circles) for soil CO_2 efflux, soil heat flux, soil temperature and Self-Potential. Red dashed lines indicate recent eruptive fissures in the area. Map Data: ©2023 Google; c) Detailed map of the North-East Rift study area, with location of sampling sites (yellow circles) for soil CO_2 efflux, soil heat flux, soil temperature and Self-Potential. Red dashed lines indicate the 2002 eruptive fissures. The blue-squared boxes indicate the areas of magnetic surveys. Map Data: ©2023 Google. Elevations in m a.s.l.

other gases from high-flow and high-enthalpy hydrothermal regions, at both high and low altitudes. In any case, these studies contributed to our understanding of the internal structure of small-scale hydrothermal convective cells. In particular, a small but well-developed hydrothermal area was subjected to detailed study in the uppermost part of the SR in the vicinity of the summit craters, at an altitude of approximately 3000 m a.s.l., with a dense grid of measurement points for self-potential, gravity, heat flux, and CO_2 efflux (Maucourant et al., 2014). In light of the intriguing findings, our objective was to employ a comparable interdisciplinary methodology to quantify the aforementioned parameters on a considerably larger scale and across a more extensive range of the two principal rift zones of Mt. Etna (i.e., SR and NER). This approach was mainly designed to elucidate potential active hydrothermal circulation at shallow depths and to examine its relationship with the structural settings and eruptive activity of the volcano. Furthermore, it was also intended to identify suitable locations for the future high-frequency temporal monitoring of the studied signals, with the aim of forecasting volcanic activity.

2. Study areas

The selected areas for survey are situated at intermediate altitude across the SR and NER (approximately 1800-2000 m a.s.l. and 2400 m a.s.l., respectively). The selection was based on the presence of observable steam emissions at the surface (in the NE rift area), the results of previous data on hydrothermal fluid circulation, and the existence of roads and tracks perpendicular to the main rift axis, which allowed for the straightforward implementation of measurement profiles across the main rift axis. The NER profile was considerably shorter than the SR profile due to the convergence of NER structures at the altitude where steam emissions occur, which narrows the area to a mere few hundred meters in width (Neri et al., 2011).

2.1 South Rift area

The SR occupies a significant portion of the southern flank of Mt. Etna, extending for about 21 km from the vicinity of the summit craters (where, on numerous occasions, eruptive fissures have originated at an altitude of approximately 3,100 m a.s.l.) down to an altitude of approximately 400 m a.s.l. (Branca et al., 2011). In the past 25 years, flank eruptions have occurred along this rift on three occasions: in 2001, 2002-2003, and 2018. It is noteworthy that in 2002-03, eruptive fissures opened both along the SR and along the NER. An area with a notable concentration of eruptive fissures is situated in close proximity to the Rifugio Sapienza tourist area (Fig. 1). Due to the aforementioned factors, as well as the relative ease of accessibility, our surveys were conducted along the primary thoroughfare that connects the village of Nicolosi, situated on the southern flank of the volcano, to the Rifugio Sapienza area and subsequently to the village of Zafferana Etnea, located on the eastern flank.

Measurements of self-potential (SP), soil CO_2 efflux, and soil heat flux were conducted on September 21 and 28, 2017, along a 4.4 km-long profile that traversed multiple historical eruptive fissures (1776, 1892-East, 1892-West, 1910, 2001), with a sampling interval of 50 m for all selected parameters (Fig. 1). A magnetic survey was conducted during the same period over a larger area across the easternmost part of SR. Prior studies on the recognition of hydrothermal activity in this area (Massenet and Van Ngoc, 1985; Aubert et al., 1984) were conducted across the upper portion of the 1892 eruptive fissure, situated just above our profile. These studies revealed a self-potential anomaly associated with a relatively deep but active hydrothermal circulation along the main fissure axis. On July 7, 2018, we conducted a follow-up measurement campaign along the eastern portion of the 2017 profile (approximately 2 km in length), reoccupying the same measurement points that were surveyed in 2017. No magnetic survey could be carried out in this occasion.

2.2 North East Rift area

The North East rift zone, as delineated by the eruptive vents, extends for about 7 km from an altitude of 2480 m a.s.l. down to approximately 1200 m a.s.l. (Branca et al., 2011). The frequency of eruptions along the NER is comparatively lower than that observed along the SR. Indeed, over the past 25 years, only one eruption has been documented on the NER, which occurred in 2002.

Our surveys, which included measurements of soil CO_2 efflux and soil heat flux, were conducted along the dirt road that connects the touristic area of Piano Provenzana (approximately 1800 m a.s.l.) to the INGV volcanological observatory located at Pizzi Deneri (2820 m a.s.l.). Two parallel profiles of measurement points, each approximately 350 m in length and separated by approximately 50 m, were conducted on July 30, 2017 along the road that traverses the NER at an almost perpendicular angle (average elevation of approximately 2470 m a.s.l.) (Fig. 1c). In contrast, a single profile of measurements was conducted on July 17, 2018, encompassing the same points as in 2017. In all cases, the sampling interval for all parameters was maintained at approximately 20 m. A magnetic survey was conducted in 2020 over an irregular grid of approximately 0.1 km², including the two profiles. The easternmost portion of the profiles traversed the upper extent of the 2002 eruptive fissure, as documented by Acocella and Neri (2003). Since the conclusion of the 2002 eruption, persistent visible surface steam emissions have been observed within the uppermost and southwesternmost crater belonging to the 2002 eruptive fissure (i.e., the first to open in the series of vents formed during the initial day of the eruption). The unusual persistence of steam discharges at the surface in this area, many years after the 2002 eruption, provides evidence that the hydrothermal system is stable and deep-rooted. This observation drove our decision to conduct our surveys at this site. Additionally, low-temperature ($T < 50$ °C) fumarole emissions are present in the same region, situated along the upslope continuation of the NE Rift at an altitude ranging from 2475 to 2550 m a.s.l.. Prior to the 2002 eruption, these fumaroles were observed to emit steam in a visible manner. However, subsequent to the eruption, only diffuse emissions that are not visually discernible have been documented (Diliberto et al., 2018). Gemmellaro (1858) documented the existence of several fumaroles in an area situated at an altitude marginally higher than that of the site under investigation in the present study. The Etna volcanological guides date the presence of these fumaroles back to at least 1911. The emissions were sampled on multiple occasions over the past 25 years, and the gases were subjected to chemical and isotopic analysis (Giammanco et al., 1999; Pecoraino and Giammanco, 2005). This revealed that the CO_2, H_2, and CO were of magmatic origin.

3. Methods

Soil CO_2 efflux, soil heat flux and self-potential surveys were carried out on 30 July and on 21-28 September 2017 along profiles of sampling points across both the SR and the NER. Measurements were then repeated on 12-18 July 2018 in most of the 2017 sites. To better define the main structural features of the investigated areas, two magnetic surveys were carried out in 2017 over the SR profile and in 2020 over the NER profile. Besides imaging processes that induce bulk mass/density changes, gravity variations can develop due to shallow processes involving the accumulation and transport of hydrothermal fluids (Gottsmann et al., 2006; Federico et al., 2023). Therefore, gravity data were taken from the routine measurements carried out with quasi-monthly frequency in different sectors of Mt. Etna volcano (Greco et al., 2022) within the volcanic monitoring activities of the Istituto Nazionale di Geofisica e Vulcanologia-Osservatorio Etneo (INGV-OE). By integration of all the parameters measured, useful information was acquired in order to define both the spatial extent and the temporal evolution of the investigated hydrothermal activity, especially in the SR area.

3.1 Soil heat flux

Values of soil heat flux were calculated after measuring the thermal conductivity of the ground, using the non-steady-state method (Bruijn et al., 1983; Bristow et al., 1994; van Haneghem et al., 1983; van Loon et al., 1989). Thermal conductivity was measured using a needle-shaped probe (Thermal Properties Analyzer, mod. KD2, Decagon Devices, Inc., USA), consisting of a heating wire and a temperature sensor, inserted into the soil to a depth of 6 cm. Values of thermal conductivity are expressed in W m^{-1} $°C^{-1}$. These data were then used to compute the one-dimensional heat flux density (in W m^{-2}) at each measurement site by means of the basic Fourier's law:

$$q = -k\,\mu z \tag{1}$$

where k is the thermal conductivity and μz is the temperature gradient along the vertical direction z, measured with a thermocouple both at ground surface and in the soil at 6 cm depth. Ninety-three heat flux measurements were

carried out along the SR profile in 2017, whereas fifty measurements were made in 2018. Thirty-six measurements were carried out along the two parallel NER profiles in 2017 and eighteen in 2018, along one profile only.

3.2 Soil CO_2 efflux

Measurements of CO_2 efflux from soil and steamy ground were performed applying the method of the dynamic accumulation chamber (Farrar et al., 1995; Chiodini et al., 1998), using a portable non-dispersive infrared (NDIR) CO_2 analyzer (model EGM-4, PPSystems, USA) provided with microprocessor control of linearization and IR cell measurement range of 0-10,000 ppm vol. Accuracy was <1% of span concentration over the calibrated range and linearity drift was <1% throughout the measurement range. Values are in g m^{-2} d^{-1} and the average error of the method is about ±5% (Giammanco et al., 2007). Ninety-nine flux measurements were carried out along the SR profile in 2017, whereas forty-nine were made in 2018 along part of the same profile. Across the NER, two parallel profiles were surveyed in 2017 with thirty-six measurements, whereas only one profile was surveyed in 2018 with nineteen measurements carried out.

The short duration of soil CO_2 surveys on both rift zones (one day on the NER, two days on the SR) prevented significant environmental effects on our measurements, mostly from air temperature and barometric pressure (Giammanco et al., 1995; Bruno et al., 2001; Granieri et al., 2003; Aiuppa et al., 2004; Viveiros et al., 2008; Cannata et al., 2009; Carapezza et al., 2009; Giammanco and Bonfanti, 2009). Environmental parameters on Mt. Etna typically vary according to annual cycles. Most typically, these cycles induce increased soil CO_2 emissions during the summer, due to a combined effect of greater biogenic activity in the soil during the warm season, increased soil permeability due to enhanced evaporation of pore water and possibly also thinning of the local underground water table (Giammanco et al., 1995; Aiuppa et al., 2004; Giammanco and Bonfanti, 2009). In the case of the present study, however, the high altitude of our measurement sites and the rather extreme conditions in the soil environment along our NER profile explain the complete absence of both vegetation and biological activity in the soil, which rules out any contribution from biogenic CO_2 to the efflux of this gas from soil. Similar conditions affect most of the SR profile, especially along its uppermost portion. Furthermore, due to the high altitude of our profiles, the local water table is deeper than 500 m below the surface (Ferrara and Pappalardo, 2008; Branca and Ferrara, 2013), therefore any effect of water level variations on soil degassing should be negligible. Conversely, changes in Mt. Etna's activity have a strong impact on diffuse CO_2 emissions, because the CO_2 emitted from the volcano's flanks is largely derived from progressive degassing of upward-migrating fresh, gas-rich magma (Giammanco et al., 1995; Bruno et al., 2001) and/or from degassing of local hydrothermal systems (Maucourant et al., 2014; Napoli et al., 2020).

3.3 Self Potential

The Self Potential (SP) method, based on the measurement of natural electric signals in a soil, has proven to be an efficient geophysical method for studying hydrothermal systems in volcanic environments (Revil et al. 1999; Hashimoto and Tanaka, 1995; Maucourant et al., 2014; Grobbe and Barde-Cabusson, 2019; Napoli et al., 2020). In volcanic areas, positive SP anomalies are generally observed where there is a strong migration of magmatic/hydrothermal fluids near the surface (Jackson et al., 1987; Lénat, 2007; Zlotnicki et al., 1998), whereas negative SP anomalies are detected in areas of infiltration of meteoric water and hence characterized by downward motion of cold fluids in the ground (Villasante-Marcos et al., 2014; Zlotnicki et al., 1998; Finizola et al., 2002, 2004; Lénat, 2007). Furthermore, drops in the SP signal, called Rapid Fluid Disruption effect (Johnston et al., 2001), may occur because: i) the geologic medium is very dry; ii) sediments are not compacted (e.g., they consist of loose tephra); iii) soil temperature exceeds 80°C. In the present study, soil temperature values did not exceed 80°C, but the other conditions were observed in many places.

On Mt. Etna, SP measurements were carried out over the SR and NER areas using a pair of $Cu/CuSO_4$ non-polarizing electrodes (developed in the laboratory "Magma and Volcano" of Clermont-Ferrand) connected with a 400 m-long graduated copper cable with benchmarks. A high-impedance multimeter (sensitivity of 0.1 mV, internal impedance of 100 MW) was used for measuring SP values between two consecutive points. Each measurement point was georeferenced by a GPS receiver. Electrodes were placed along the SR profile at 50 m intervals for a total distance of about 5 km, whereas for the NER electrodes were set up in a loop configuration, making a grid with a step of 20 m

(Fig. 1). A good contact between electrodes and soil was guaranteed by the presence of homogeneous and incoherent volcanic deposits, mainly ashes and scoriae. In each survey, the so-called reference electrode was placed in the ground at depth of 5-40 cm, as far as possible from the hydrothermal area and in an area of stable SP values. In the shorter 2018 survey, point P35 was set as a reference point (with absolute value of 445 mV). The Kirchoff law was used to remove the drift of electrodes signals inside the loop of measurements covering the NER area (Revil and Jardani, 2013; Villasante-Marcos et al., 2014), whereas for the SR profile we measured the drift in each line of 400 m. All SP measurements showed a high accuracy, with drift less than 10 mV as measured at the end of each profile or loop of electrodes within the same profile.

SP measurements in these survey areas were not significantly affected by the elevation effect, because along the NER all profile benchmarks were located at approximately the same elevation (about 2500 m a.s.l.) and along the SR profile the difference in elevation between the start and finish points was only about 200 m (from 1700 to 1900 m a.s.l.) over a 4.8 km – long profile, thus not enough to cause this effect (Villasante-Marcos et al., 2014).

3.4 Magnetic Survey

On Mt Etna the strong magnetization contrasts generated by the presence of rocks with different magnetic properties make the magnetic method and the related magnetic anomaly maps a valid tool for structural investigations (Del Negro and Napoli, 2002; Nicolosi et al., 2014; Napoli et al., 2020, 2021). Therefore, two magnetic surveys were carried out, in 2017 and in 2020, across the profiles surveyed for the other parameters. The 2017 survey covered an area of about 1.3 km^2 centered on the 1892 eruptive fissure (Fig. 1b), with more than 5500 data gathered in a time span of 2 days. The 2020 survey was carried out over a surface of about 0.1 km^2 (Fig. 1c) across the NER zone, with 3500 data acquired in one day. In this case, the 2002 eruptive fissures were only partially included in the survey because the 2002 lava flows prevented from reaching the terrains located east of the eruptive fissures.

In order to reduce background noise, the magnetic sensor was placed on an aluminum pole, 2 m above the ground. Magnetic data were collected by a GSM19 Overhauser effect magnetometer (0.01 nT resolution) along a network of profiles describing irregular grids crossing the profiles surveyed for the other parameters considered in this study, with spacing of about 3 m. Simultaneously, GPS data were also gathered to geo-reference magnetic measurements. The time variations of external origin were removed using data continuously recorded at the nearest magnetic stations of the permanent network for magnetic monitoring of Mt Etna (Napoli et al., 2008), that in our case were CST – located about 2 km north of the SR profile – and PDN – located about 2 km south of the NER. After a data reduction process, whose details can be found in Napoli et al. (2020), magnetic data were reduced to an equally spaced grid using the Kriging method. Before relating magnetic anomalies to volcanic and/or tectonic features, we applied the reduction to the pole transformation (RTP) to the diurnally corrected data, in order to minimize the dipolar nature of the measured magnetic field. RTP, indeed, transforms each dipolar anomaly into either a negative or a positive anomaly, whose shape is more closely related to the spatial location of the source geometry (Baranov, 1957), thus allowing for a readier determination of the location of magnetic sources. In order to produce the RTP map we applied a magnetic inclination of 53°N and a magnetic declination of 3.4°W, that are equal to the present-day Earth's field direction in the place of the survey. Actually, Etna volcanic rocks (about 0.5 Ma; Gillot et al., 1994) were emplaced after the last planetary magnetic field reversal (0.78 Ma; Lowrie and Kent, 2004) and their residual magnetization is generally more intense than the induced magnetization (Königsberger ratio is >1; see e.g. Tric et al., 1994; Branca et al., 2019).

3.5 Gravity Survey

Evidence for a hydrothermal contribution to gravity signals on different time scales has been found in several cases around the world (Gottsmann et al., 2005; 2007; Berrino 2000; Todesco and Berrino, 2005; Tikku et al., 2006; Di Maio and Berrino 2016; Federico et al., 2023). Gravity measurements are typically repeated over time, either in large-scale surveys or in continuous mode at fixed locations, to estimate how the gravity field has changed at a single point or along an array of fixed observation points during the interval between successive surveys.

At Mt. Etna, gravity measurements have been accomplished since the 1980s, allowing shedding light on the volcanic processes occurring in the shallow and intermediate plumbing systems of the volcano (Carbone et al., 2009, 2014;

Carbone and Greco, 2007; Greco et al., 2010, 2012, 2016, 2022; Del Negro et al., 2013). Since the installation of the gravity network on Mt. Etna (Budetta et al., 1989), which currently consists of 80 benchmarks, field gravity measurements have been performed on a monthly basis using Scintrex relative gravimeters. The network is linked to a reference station where absolute gravity measurements have been performed since 2007 (Greco et al., 2012; 2022).

Comparison of data between consecutive surveys at Mt. Etna performed since 1995 (Budetta et al., 1999) revealed, in some periods, cyclic gravity variations in different sectors of the volcano.

4. Results

4.1 South Rift area

The 2017 measurements across the SR showed large spatial variations of all parameters surveyed (Fig. 2a). Along the main W-E profile, soil temperature values ranged from 2.7 to 32.0 °C and the associated heat flux values ranged from −36.8 to 28.5 W m^{-2}; soil CO_2 efflux values varied from −9.8 to 35.5 g m^{-2} d^{-1} and SP values ranged from 0.2 to 594.0 mV. Figure 2a shows that the surveyed profile can be divided into two distinct portions, each with a well-defined behavior of the three parameters above. The westernmost part of the profile (points 1 to 35) showed lower average values both of soil heat flux (with many negative values) and of SP, whereas soil CO_2 effluxes were higher on average and reached their maximum value at point 2. The east part of it (points 35 to 99) showed an almost opposite behavior, with higher heat fluxes and SP values and highly variable soil CO_2 fluxes (ranging from negative values to remarkably high ones).

In order to define anomalous levels of both CO_2 efflux and of soil heat flux, the probability-plot technique (Sinclair, 1974) was applied to the entire data sets. A Lognormal probability graph was constructed with the CO_2 efflux data to recognize the presence of overlapping different statistical populations (Fig. 3a). The resulting probability graph allowed us to distinguish six populations (from A to F in Fig. 3a) and to separate them from the original CO_2 efflux data set. Populations A and B, together representing 40.8% of the total data, were characterized by negative or zero values, which is explained in terms of downward flux of CO_2 due to draining of CO_2 from air into the ground caused by downward convective motion of hydrothermal fluids. Populations C and D, together representing 39.8% of the total data, showed efflux values lower than 8 g m^{-2} d^{-1} and, therefore, they would represent the normal background degassing due to a pure biogenic contribution to the soil CO_2 efflux. Such low values compared to other areas of Mt. Etna (normally, the upper limit for background soil degassing was set at about 70 g m^{-2} d^{-1}, Giammanco et al., 2007) is explained by the limited diffusion of plants and biogenic activity in soil in the study area because of both the high altitude and the widespread cover of recent lavas. Actually, the average value of CO_2 efflux in areas characterized by scarce vegetation, uncultivated meadows, mediterranean maquis or semiarid steppe was 7.6 g m^{-2} d^{-1} (Angell et al., 2001; Frank et al., 2002; La Scala et al., 2000; Maestre and Cortina, 2003; Mielnick and Dugas 2000; Obrist et al., 2003; Raich and Schlesinger, 1992; Raich and Tufekcioglu, 2000; Reth et al., 2005), very close to the upper limit of biogenic degassing found in our area. Population F, representing 11.2% of the total data, would then represent the peak degassing (efflux >8 g m^{-2} d^{-1}) due to upward (likely advective) motion of hydrothermal/magmatic CO_2 (Hernández et al., 2001).

The normal probability plot constructed with the soil heat flux data from the 2017 survey (Fig. 3b) allowed us to recognize and distinguish six different populations (from A to F). In this case, increasingly higher heat flux values, in particular those higher than 7.2 W m^{-2} (populations D to F in Fig. 3b), suggest a progressive greater input of high-enthalpy fluids from hydrothermal systems.

All three parameters above showed in general their highest values mostly between points 52 and 93 in the 2017 profile (Fig. 2a), that is where the profile crossed the main recent eruptive fissures of the SR (Fig. 1). Furthermore, Fig. 2a clearly highlights several large SP positive (high increasing signal) anomalies, the largest of which are located along the axis of the two 1892 eruptive fissures (easternmost portion of the SR profile) and in between the ideal continuations of the 1910 fissure and of the Mt. Vetore fissure (central-western portion of the SR profile). The sharp increase of values (about 300 mV) observed between sites P8 and P19 would thus mark the west limit of the main hydrothermal cell in the SR of Mt. Etna. Other smaller positive anomalies were observed in the central part of the same profile.

In between the high SP values, several relatively low values were measured, thus indicating alternation of several convective cells of “hot” fluids, whose upward motion causes the positive SP anomalies and whose downward

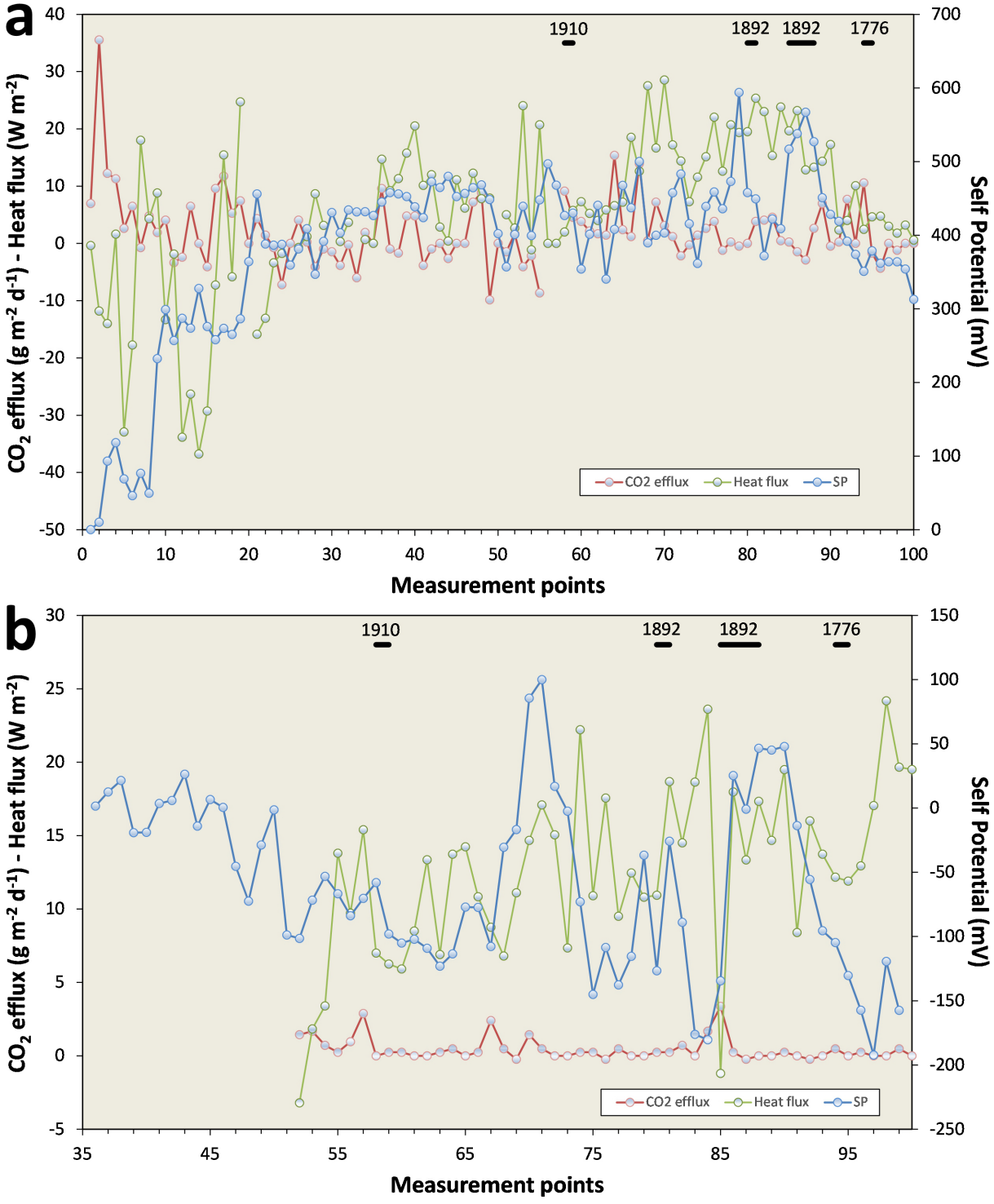

Figure 2. Spatial distribution of values of soil CO_2 efflux (red dots and lines), soil heat flux (green dots and lines) and Self-Potential (blue dots and lines) along the profiles surveyed across the South Rift study area in (a) 2017 and (b) 2018. In the 2018 survey, measurements were repeated only from point P34 to point P97 and the value of 445 mV (taken at P0 = P35 in 2017) was considered as reference for SP measurements. On top of the plot is shown the position of the main recent eruptive fissures that cross or end close to the profile.

motion causes the negative (high decreasing values) ones. In general, the most intense SP positive anomalies (several hundreds of mV) on volcanoes were found in active degassing fracture zones or in fumarole areas (with hydrothermally altered rocks) associated with presence of large amounts of hot water (or steam) in the subsurface (Jackson and Kauahikaua, 1987; Hashimoto and Tanaka, 1995; Zlotnicki et al., 2003; Finizola et al., 2004; Lénat

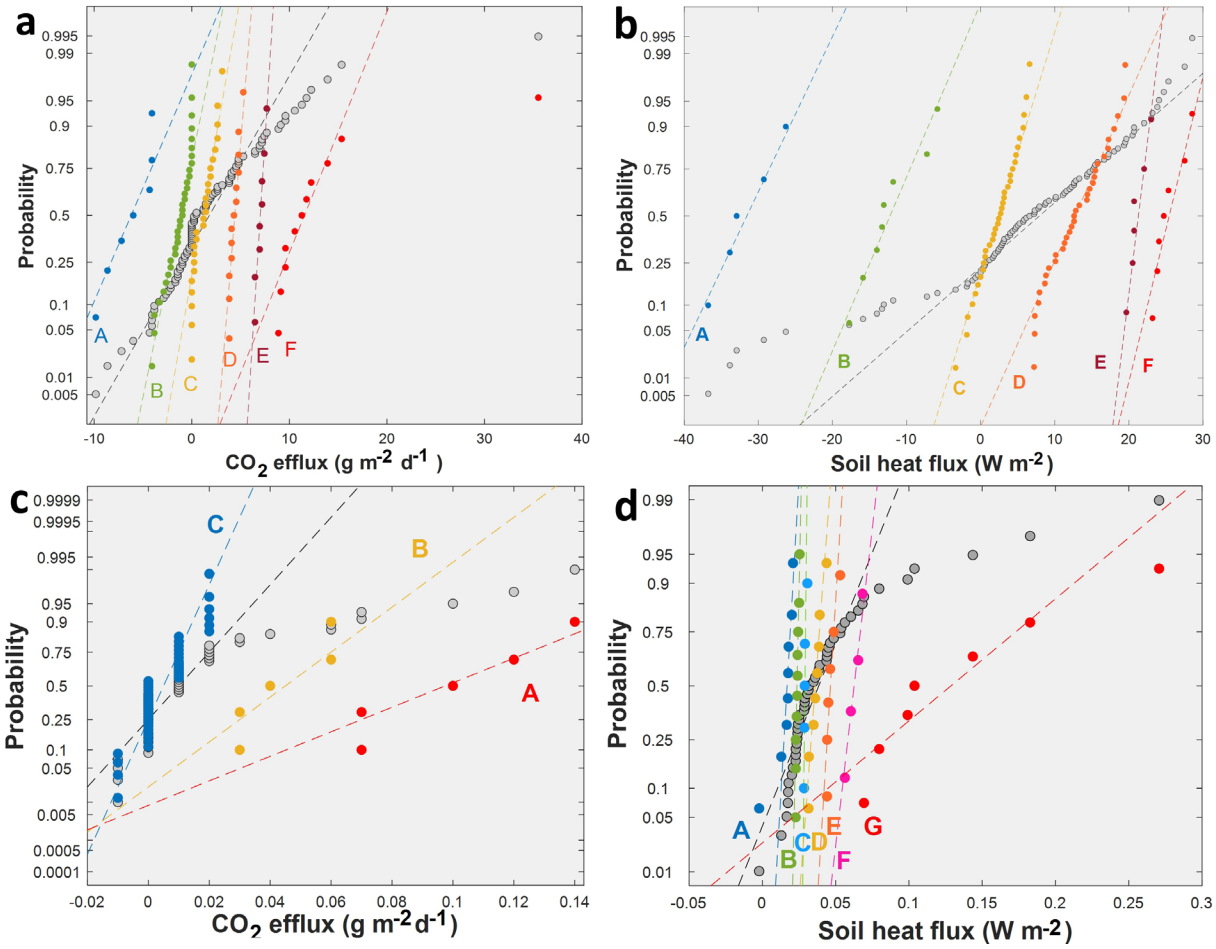

Figure 3. Normal Probability Plots for the values of (a) soil CO_2 efflux measured in 2017; (b) soil heat flux measured in 2017; (c) soil CO_2 efflux measured in 2018 and (d) soil heat flux measured in 2018 along the South Rift profile. On this type of plot, a single uniform statistical population of data will be shown as points falling on a straight line. According to Sinclair (1974), changes in the slope of the lines of points indicate separate populations of data. In all plots, the original data are indicated with gray circles, whereas sub-populations of data are shown with color circles and capital letters. In plot (a), six populations of CO_2 effluxes were recognized, describing progressively higher effluxes with increasing contribution from magmatic/hydrothermal CO_2 (from A to F). In plot (b), six populations of soil heat fluxes have also been identified, describing progressively higher heat fluxes with increasing contribution from high-enthalpy hydrothermal fluids (from A to F). In plot (c) three populations of CO_2 effluxes have been recognized, describing progressively higher effluxes with increasing contribution from magmatic/hydrothermal CO_2 (from A to C). Finally, in plot (d) seven populations of soil heat flux data have been recognized, with increasing contribution of heat from high-enthalpy hydrothermal fluids (from A to G).

2007). The geometry of the anomalies observed in the above parameters along the east part of the SR profile seemed, therefore, to indicate a large hydrothermal body (located between points 35 and 88 of the SR profile) characterized by many smaller convective cells. The central part of this hydrothermal body was characterized mostly by ascent of condensed steam, which justifies the high heat flux and the high ground conductivity. Besides, in several points we observed a drift of a few mV during SP data acquisition (drift in mV: P83 = 7; P84 = 12, P85 = 9, P86 = 7, P87 = 6), which is due to active motion of groundwater near the surface (Aubert et al., 1984; Maucourant et al., 2014). It is noteworthy that the highest SP values were measured on the 1892 fissures, very close to where a similar positive anomaly was observed by Aubert et al. (1984), who interpreted it as due to flux of ascending steam that condensates at depth >6 m. Given the large width of the highest SP anomaly near the 1892 fissure (about 400 m), the hydrothermal cell detected must extend to a depth of at least several hundreds of meters.

Looking more in detail at the spatial distribution of soil CO_2 effluxes along the east part of the SR profile, we noticed that the highest soil effluxes were measured in particular at points 57-68 and 87-92, that is almost at the edge of both the largest thermal anomaly and the highest SP values. Furthermore, markedly negative CO_2 efflux values were recorded just west of the large zone of high SP and heat flux values, reaching their lowest values at points 49 and 55 of the profile. The emission of CO_2 is in general not very high in the central part of the presumed hydrothermal cell (i.e., between point 68 and 87). This is probably due to partial dissolution of the deep-sourced gas into liquid water that had formed by condensation of ascending steam in the layers of ground located, at most, a few hundreds of meters below the surface. On both sides of this anomalous zone, very high emissions of CO_2 gas occurred due to the lower amount of condensed steam in the ground and hence to lower dissolution of CO_2 into the liquid phase. Negative efflux values are indicative of influx of CO_2 from the atmosphere into the soil. It is the first time that such negative fluxes were found on Mt. Etna. Similar negative values were previously observed only in arid and semiarid regions and they were explained as due to biogenic intake, to pH-controlled dissolution of inorganic CO_2 into saline/alkaline soils and/or to basalt and carbonate weathering (Ma et al., 2015; Wang et al., 2015; Cueva et al., 2019). In the case of the east portion of the SR profile, given the absence of vegetation and the obvious lack of carbonate rocks in the near-surface environment, such negative CO_2 fluxes are likely due to influx of atmospheric gas induced by the downward motion of fluids along the descending side of the large hydrothermal convective cell described above.

The measurements across the SR were performed again in 2018 along a reduced extension of the profile (64 points out of the original 100 were surveyed for SP, whereas only 50 out of 100 were surveyed for soil heat flux and soil CO_2 efflux). Soil temperature values ranged from 17.7 to 40.3 °C, soil heat flux values ranged from –3.20 to 0.27 W m^{-2}, soil CO_2 efflux values varied from –0.24 to 3.36 g m^{-2} d^{-1} and SP values ranged from –192.2 to 100.0 mV (252.8 to 545 mV after referring the zero value to the reference points P0, P35 in 2017). In general, the intensity of all three parameters was markedly attenuated compared to the results of the 2017 survey (Fig. 2). Both the SP and the soil heat flux maxima roughly corresponded with those of 2017, particularly across the 1892 fissure. However, new high values of heat flux appeared on the easternmost end of the 2018 profile, approximately along the axis of the 1776 eruptive fissure. Similarly, high values of SP appeared in 2018 between the 1910 and 1892 eruptive fissures, whereas high SP values were strongly diminished along the west part of the 1892 fissure. Soil CO_2 effluxes were in general very low and close to background values, with some small anomalies located almost exclusively along the east part of the 1892 eruptive fissure and close to the 1910 one, similar to what was found during the 2017 survey. The Log-normal probability graphs for both soil CO_2 efflux and soil heat flux data collected in 2018 (Figs. 3c, d) confirmed the above observations, because the largest majority of data belonged to background populations.

From the above data, it seems that the large convective cell found in 2017 still existed in 2018, but its intensity was sensibly lower, it was less continuous in its lateral extension across the SER and it was mostly confined to the easternmost part of the profile. From the 2018 SP and heat flux data it seemed that the eastern edge of the main convective cell had extended further to the east of the 1892 fissure, thus closer to the 1776 fissure. By comparing the results of the two surveys of 2017 and 2018, therefore, the 1892 fissures seemed to host the most stable part of this large hydrothermal body along the SR. The appearance in 2018 of more pronounced anomalies centered on point P68 better highlights a smaller convective cell between the 1910 and 1892 eruptive fissures, more specifically between points P66 and P76, which was not as evident in the 2017 survey.

As regards the results of the magnetic surveys, the total-intensity anomaly fields measured in 2017 were quite articulated, being characterized by anomalies with variable spatial extension and variable intensity (Fig. 4a). The RTP map related to the SR zone (Fig. 4b) reveals two intense and well-defined maxima striking South-North, located along the 1892 eruptive fissure and reasonably associated to the main feeding system of that eruption. In between the two maxima, a low magnetization area is revealed between P84 and P87 measurements points. Moreover, a wider magnetic low is observed in the area surrounding the Rifugio Sapienza hut in the western part of the investigated area, between P66 and P71 measurements points. Both of the magnetic lows are located in correspondence of the areas characterized by the highest values of SP, CO_2 efflux and soil heat flux. These magnetic signatures could be related to an alteration of the local rocks' magnetization, thus supporting the presence of a preferential way for upward migration of hydrothermal fluids to the surface. However, the temperature values recorded in 2017 and 2018 are not high enough to produce a demagnetization process, as temperatures higher than 500°C are generally required, so we cannot rule out that this process was produced by past hydrothermal activity.

In the SR area, gravity measurements over time revealed cyclic changes over months-long periods, without a noticeable ground deformation associated (Bonforte et al., 2017). For the sake of reinforcement, we report here

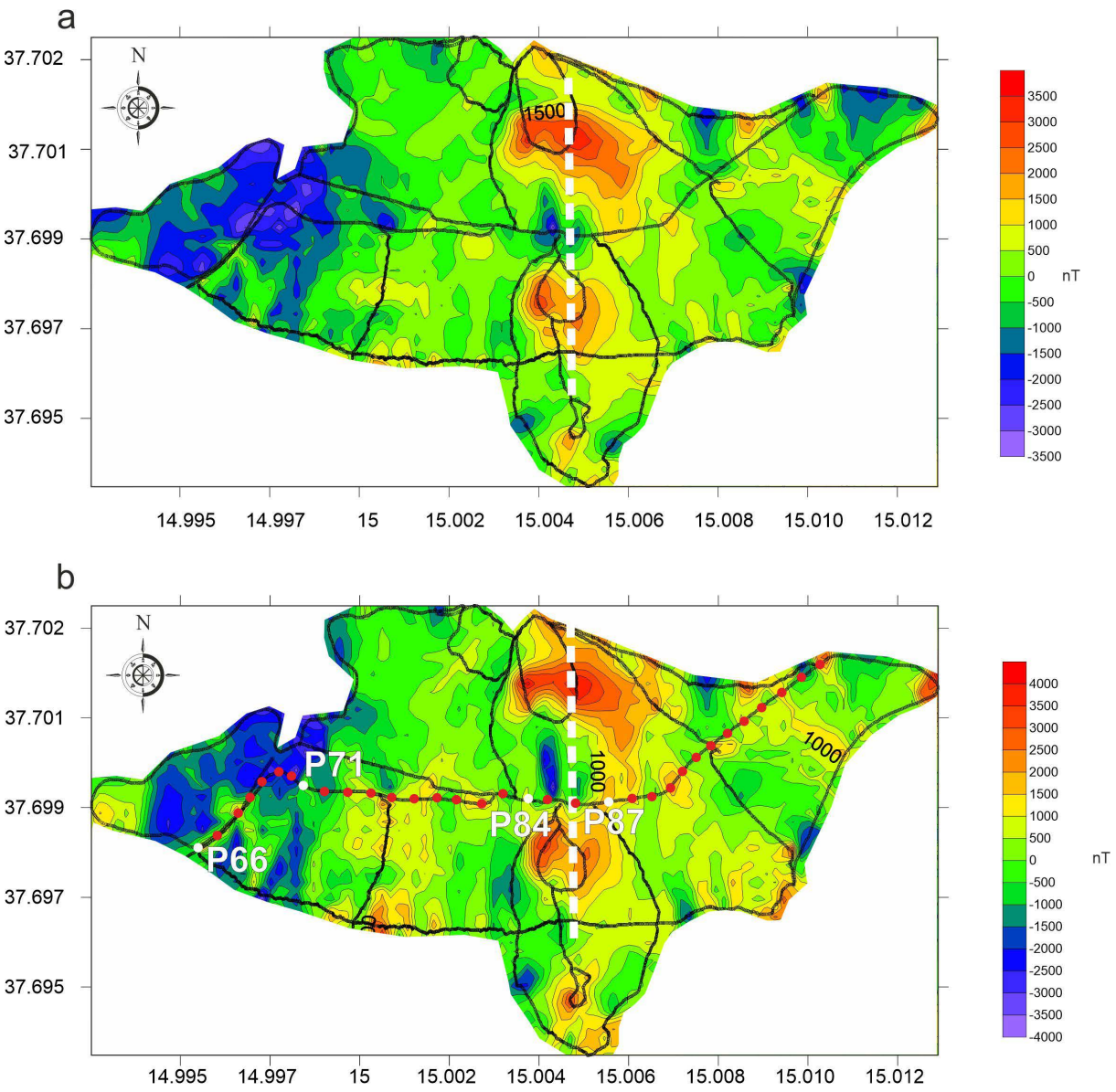

Figure 4. (a) Total field magnetic anomaly map across the South Rift study area; (b) Map of the reduced-to-the-pole magnetic data in the same area, with the location of the measurement points of soil CO_2 efflux, soil heat flux, soil temperature and Self-Potential (red dots). The black lines indicate paths of magnetic measurements, whereas the white dashed lines show the 1892 eruptive fissure.

the gravity changes observed between 18 November 2020 and 28 May 2021, even though they are temporally spaced from the other surveys conducted in 2017 and 2018. During this period a gravity increase was observed between 18 November 2020 and 09 March 2021, with maximum amplitude of about 50 microGal measured in the stations CL and CM (Fig. 5). Subsequently, a decrease in gravity with the same amplitude and affecting the same stations was observed between 09 March 2021 and 28 May 2021 (Fig. 5b). Given the similarity in terms both of spatial pattern and of amplitude of the gravity changes between the phases of increase and decrease, we assume that the processes driving the changes observed during the whole interval considered developed within the same source volumes and that similar mass and volume changes were involved during the two sub-intervals, although with opposite sign. Gravity changes were inverted to constrain only the source location. The inferred mass-source model is centered slightly east of CL and CM stations (red circle in Fig. 5a), at an absolute depth of about 1.5 km above sea level. Because of the eccentricity of the source relative to the summit craters and its shallowness (600-700 meters below the surface), it is reasonable to assume that the variations observed are not caused by shallow magma intrusions, but rather by enhanced circulation of subsurface hydrothermal fluids. More specifically, our observations can

be explained according to the model of Bonforte et al. (2017), that invoked a complex interplay between a deep (below sea level) magma chamber and a shallow (above sea level) groundwater system, which causes boiling and evaporation of the latter.

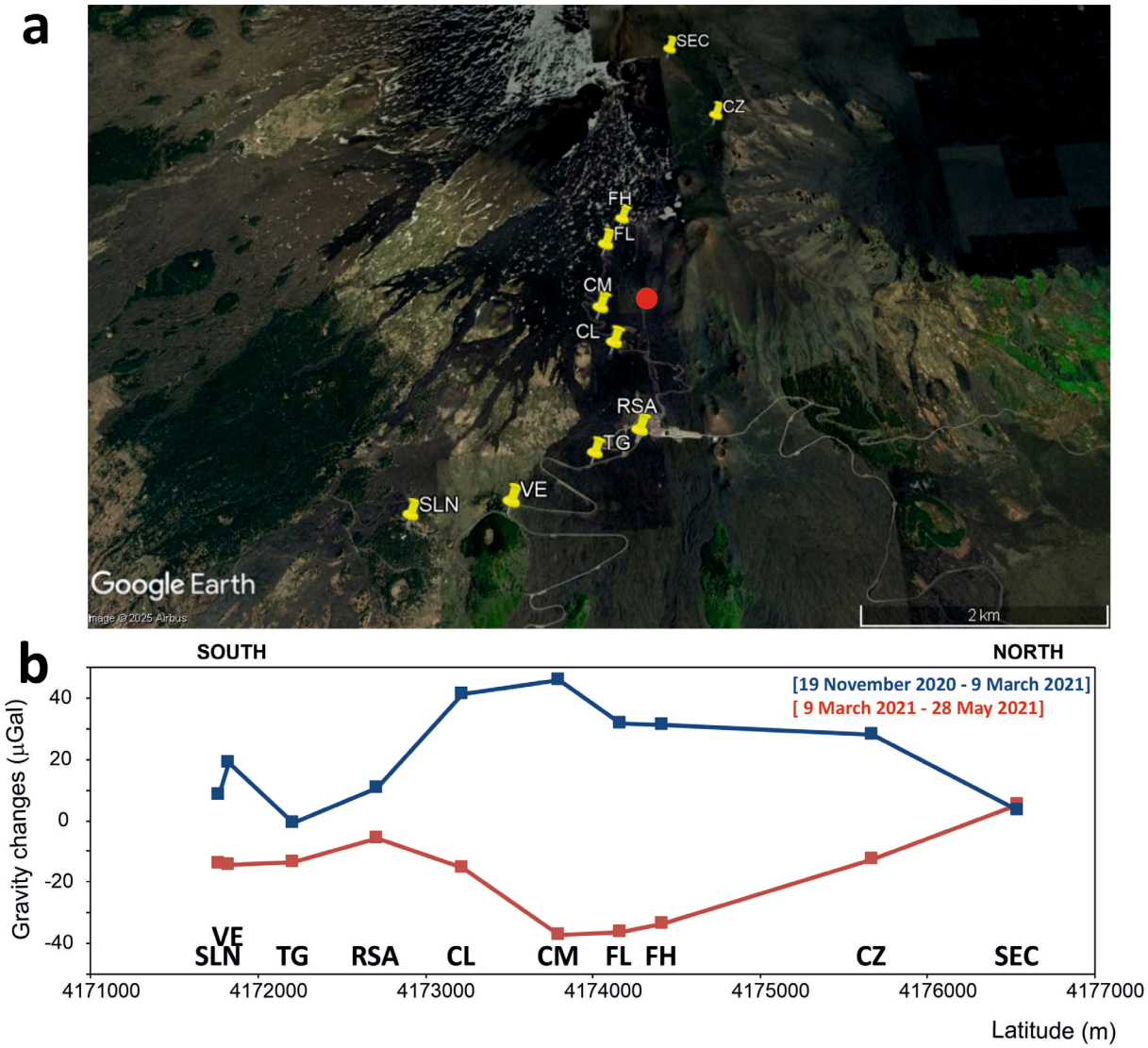

Figure 5. (a) Sketch map of the central portion of the South flank of Mt. Etna (Map Data: ©2023 Google), showing the positions of the gravity measurement stations (yellow symbols and related acronym) along the South Rift. The red circle highlights the projection on the surface of the underground source of gravity changes; (b) gravity changes observed in the above stations in the periods from 19 November 2020 to 09 March 2021 (blue line) and from 09 March to 28 May 2021 (red line).

4.2 North Rift area

During the 2017 survey across the NER profiles (Figs. 6a, b), soil temperature values ranged from 12.8 to 32.2 °C and the associated heat flux values ranged from −40.3 to 4.7 W m^{-2}; soil CO_2 efflux values varied from −5.8 to 477.6 g m^{-2} d^{-1} and SP values ranged from −71.8 to 226.7 mV. The strongest positive anomalies of all these parameters were observed almost exclusively along the SW end of the 2002 eruptive fissure, where visible steam emissions occur. Another marked positive anomaly, although limited to soil temperature and soil heat flux, was observed near the NW limit of the profile (points P1 to P5 and point P23), accompanied by a negative anomaly of SP and some relatively high values of CO_2 efflux in points nearby. The distribution of data from the above parameters

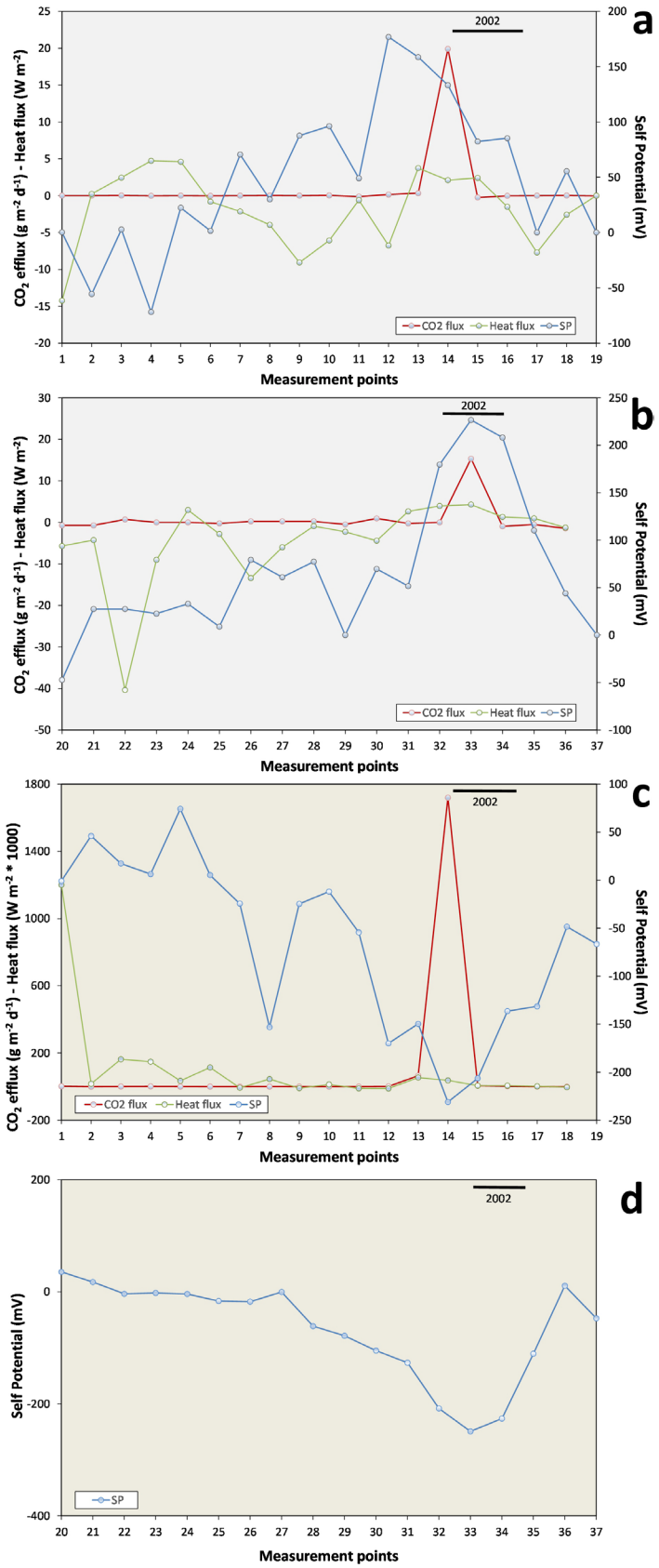

Figure 6. Spatial distribution of values of soil CO_2 efflux (red dots and lines), soil heat flux (green dots and lines) and Self-Potential (blue dots and lines) along the two profiles surveyed across the North East Rift study area in 2017 (a and b) and in 2018 (c and d). Note that heat flux values in 2018 were multiplied times 1000, in order to enhance their variations on the plot. On top of the plots is shown the position of the 2002 eruptive fissure where it crosses the profile.

strongly supports the existence of an upward motion of hot volcanic fluids beneath the uppermost vents of the 2002 eruptive fissure. These fluids eventually feed the gas emissions at the steamy fumaroles located at the bottom of the southwestern most vent. In particular, according to the SP data, either the source of the hydrothermal circulation is likely near the surface or it is located along the conduit of the 2002 vent. Therefore, the 2002 eruptive fissure,

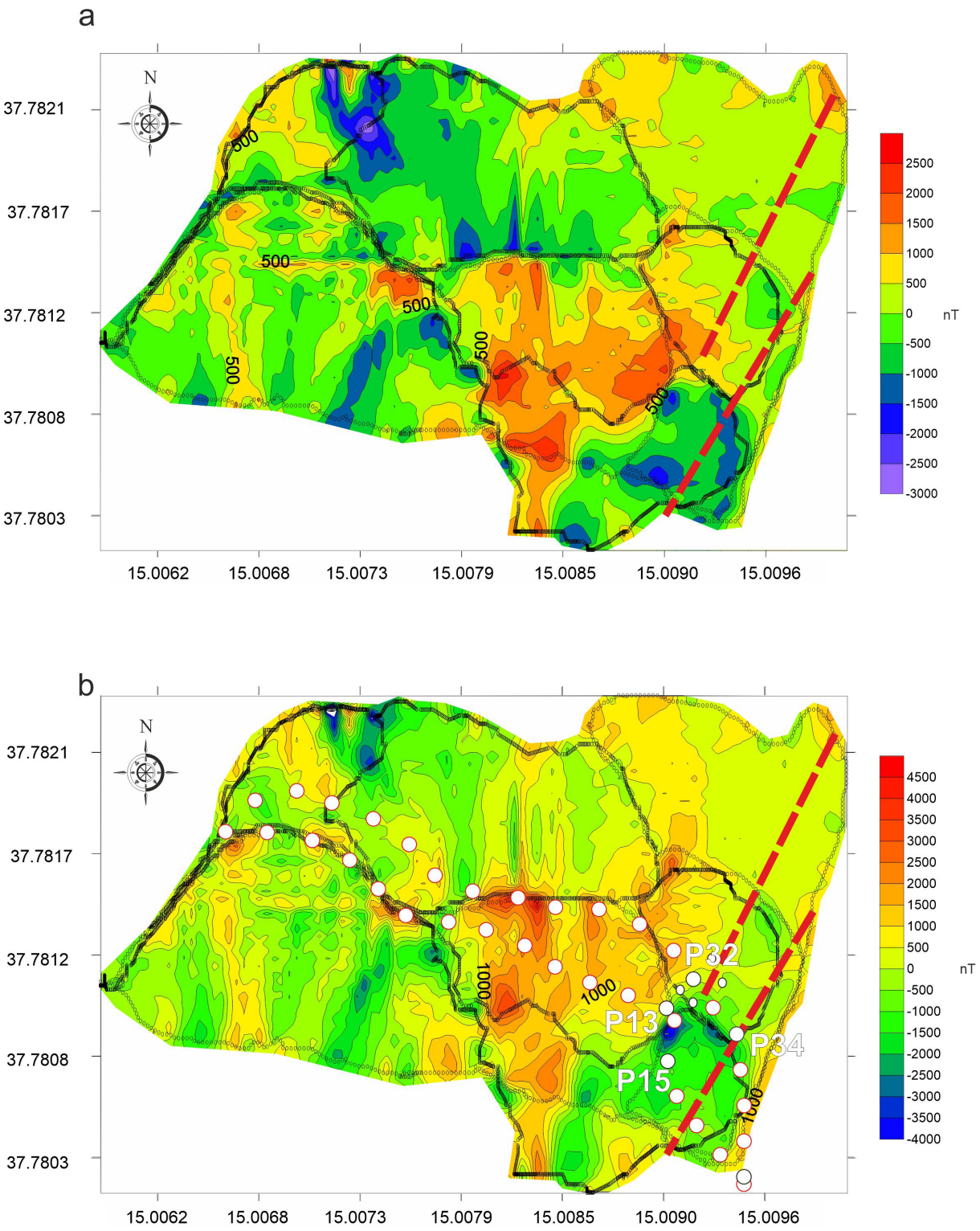

Figure 7. (a) Map of the total field magnetic anomaly across the North-East Rift study area; (b) Map of the reduced-to-the-pole magnetic data, with the location of the measurement points of soil CO_2 efflux, soil heat flux, soil temperature and Self-Potential (white dots). The black lines indicate paths of magnetic measurements, whereas red dashed lines indicate the 2002 eruptive fissures.

although extinct, would still represent a high-permeability pathway for the fast upward migration of hydrothermal fluids to the surface.

The other large positive heat flux anomaly along the profile corresponds with strong negative SP values and no significant anomaly in CO_2 effluxes. This suggests a downward motion of fluids (condensation side) in the same convective cell that produced the fumarole emissions in the east portion of the profile. The high soil heat flux in these points, therefore, would result from surface release of the latent heat of condensation produced during this process, which does not imply release of CO_2 because this gas was already totally lost by the hydrothermal fluids during their ascent.

As for the SR profile, the results of the 2018 survey along the NER profile showed a completely different situation if compared to 2017 (Figs. 6c, d). Although soil temperature values were quite similar to those of 2017, ranging from 19.7 to 28.8 °C, the associated heat flux values were on average much lower and they varied in a much narrower range, from −0.01 to 1.2 W m^{-2}. Soil CO_2 efflux values showed the largest variation, as they ranged from −0.72 to 1719.36 g m^{-2} d^{-1} and their peak was about four times higher than that measured in the previous year. SP values ranged from −231.0 to 74.2 mV and showed an opposite behavior compared to those of 2017, because the 2002 eruptive fissure was associated with a strong negative SP anomaly, indicating marked downward motion of fluids. A weak positive anomaly was instead observed on the west part of the profile.

The above data indicate that in 2018 an inversion occurred in the polarity of the convective cell that was emplaced along the upper NER, although the emission of CO_2 was higher than in 2017 and it was associated with a downward motion of cold fluids, differently from what was observed in 2017.

This evidence supports the hypothesis that the CO_2 emitted at the 2002 vent had a different, seemingly deeper, source than the other gases emitted from the local hydrothermal system. Withdrawal of hydrothermal water along the 2002 fissure in 2018 and the consequent thinning of the local hydrothermal reservoir may have strongly reduced the scavenging of CO_2 by its dissolution into the thermalized groundwater. Deep CO_2 was therefore able to reach the surface with a higher flux, leading to its stronger emission at the surface in 2018.

The magnetic anomaly map in the NER zone (Fig. 7), is quite articulated and it seems to be consistent with the lithological alternation of lava flows, pyroclastic rocks and ash present in this area. No particular spatial pattern is apparent, except in the upper eastern part of the map (i.e. corresponding to the 2002 eruptive fissures), where a low magnetization area was revealed despite the presence of recent lava flows, which are generally characterized by higher magnetization. As observed in the SR zone, the magnetic low is close to the area with the highest values of SP, CO_2 efflux and soil heat flux (measurement points P13-P15 and P32-P34).

No evident gravity variations attributable to cyclic hydrothermal dynamics were observed in the stations located along the NE Rift. This phenomenon can be attributed to the considerable spacing between gravity stations in this area (approximately 1 km) and it suggests that the hydrothermal circulation in this area is spatially confined within the spacing between two consecutive stations. This finding is compatible with the results from the other parameters described above, thus supporting the hypothesis that the local hydrothermal system is relatively small and mostly confined within the 2002 eruptive fissure.

5. Discussion of data

The role of rift zones in driving magma to its eruption at the surface is fundamental to the eruption process of basaltic volcanoes like Mt. Etna. It is therefore of paramount importance to detect the form, extension and intensity of shallow hydrothermal bodies fed by magmatic fluids along rift zones for the purposes of volcano monitoring and, ultimately, eruption forecasting. The multidisciplinary approach described in this work is, in our opinion, beneficial in these respects. This study presents, for the first time on Mt. Etna, the results of a multidisciplinary approach to the detection of shallow hydrothermal activity along rift zones of this volcano. This approach involved surveys of soil CO_2 and soil heat flux at the surface, together with surveys of self-potential, magnetism in shallow ground. Moreover, this was the inaugural instance of employing a measurement spacing of 50 m in SP surveys, thereby allowing an unprecedented detail in the detection of fluid circulation in the ground. The combination of geochemical and geophysical methods facilitated the straightforward and precise detection of convection-driven hydrothermal cells at varying scales (from a few hundred meters to several kilometers) across the SR and NER of Mt. Etna. The repetition of the surveys in different years permitted the revelation of temporal changes in the hydrothermal bodies mapped, both in terms of their size/shape and in terms of their presumed bulk volume.

Both the 2017 and the 2018 surveys clearly showed that shallow hydrothermal bodies occur in the two main rift zones of Mt. Etna. In both surveyed areas, circulation of hydrothermal fluids forms well-defined convective cells, whose lateral extension depends both on the number and on the dimensions of the fractures and faults through which fluids can flow. All of the surveyed parameters agree on the geometry of the hydrothermal convective cells existing in the two areas of investigation. Specifically, the convective motion of fluids (that, in this case, are likely composed mostly of condensed steam) is particularly well defined for the 1892 fissures in the eastern part of the SR profile and near the uppermost crater of the 2002 eruptive fissure in the NER area, where low magnetization areas, reasonably related to the hydrothermal activity, were also detected.

Along the SR, mirroring the complexity of the structural framework of the area, several hydrothermal cells were found to have developed. A main and stable convective cell is located along the 1776-1892 fracture systems, indicating constant upward migration of high-enthalpy ($T < 100$ °C) fluids along those volcano-tectonic structures. Minor convective cells seemingly appear only when the input of deep fluids is higher. The main stable hydrothermal body, therefore, would be emplaced into volcano-tectonic structures permeable enough to be constantly "open" to circulation of magmatic/hydrothermal fluids and hence connected at some depth with the main plumbing system of the volcano. Being preferential and stable pathways for the release of mass and energy from Etna's central conduit, the 1776-1892 fracture systems, detected also by magnetic data, would thus still keep all the potential for being sites of future flank eruptions along the SR. Also, the gravity changes observed along the SR are consistent with hydrothermal circulation as the causative source for the observed gravity variations and well support the interpretation of spatial-temporal changes in terms of presence of subsurface thermal fluids.

Along the NER, the 2002 eruptive fissure is clearly a major pathway for the release of mass and energy from the volcano's conduit (Donatucci et al., 2020; Falsaperla et al., 2020). Its formation seemingly altered a previous stable hydrothermal body, located about 200 m to the west, that was extensively studied and monitored before the 2002 eruption (Pecoraino and Giammanco, 2005). Gas emissions from this "old" system were found to derive from magma degassing and seemingly driven by another important, though buried, volcano-tectonic structure belonging to the NER (Pecoraino and Giammanco, 2005). The pre-2002 hydrothermal cell is still detectable from our data, as it would be responsible for the anomalies observed at points P4 and P23 of the NER profiles. It is also still observable at the surface as scattered emission of steam located some hundreds of meters uphill of our surveyed area. It is worth of note that along the NER, both stable steam emissions and gas vents occur in a well-defined area, at altitude between 2500 and 2600 m a.s.l.. This area is near to the presumed crossing between the NER and the old, partially buried rim of the Ellittico caldera, which probably occurs at about 2750 m as defined by geological and morphological observations (Branca et al., 2011). Therefore, the surveyed area could represent a significant stable weak point in the structure of Mt. Etna, thus being a preferential pathway for the upward migration both of magmatic/hydrothermal fluids and of magma intrusions coming from the deep magma reservoirs of the volcano. This would also explain why flank eruptions along the NER tend to occur below 2500 m (i.e., below the elevation of the buried Ellittico caldera rim). Unluckily, the sparse distribution of the gravity stations in the NER areas did not allow for a more detailed and certain interpretation of the results. Thus, only a qualitative description of this parameter is possible from the observed variations in this latter area. A denser network or targeted microgravity surveys would improve resolution. Another important limitation of the present investigation is that the NER profile only covers a short segment (approximately 350 metres) of the rift zone's total width. This prevents us from generalising our results or fully resolving the lateral extent of the hydrothermal system. Future studies would benefit from a broader survey area.

The marked temporal changes observed between 2017 and 2018 in both surveyed areas indicate that all of the mapped hydrothermal bodies act in a similar manner, exhibiting a high degree of sensitivity to variations in the input of mass and energy through the volcano feeder conduits. This sensitivity appears to be distributed equally and contextually across all of the mapped hydrothermal bodies, thus suggesting that the hydrothermal bodies investigated belong to a single interconnected system. The general decrease in the intensity of hydrothermal activity observed at the SR in 2018, compared to 2017, could be explained in terms of decreased input of magmatic fluids to shallow hydrothermal reservoirs caused by fast upward migration of large amounts of gas-rich magma from deeper to shallower levels of the volcano feeder system. In this case, most of the magmatic degassing in 2018 would have occurred at higher elevation than the roots of the eruptive fissures that we surveyed. This process, if proven true, was particularly strong at the NER, where it led to an inversion of the vectors of fluid flow in the hydrothermal circulation emplaced inside the 2002 eruptive fissure, indicating withdrawal of condensed fluids from shallow to deeper levels of the volcano. This seems to be a common process at Mt. Etna, as the intensity of flank degassing closely mirrors

the depth of large volumes of magma inside the volcano. As already observed in several occasions, flank degassing becomes stronger when the magmatic source of gas is deeper than the gas emission points at the surface, whereas it sensibly diminishes once magma has moved upward to an elevation higher than the depth where gas-emissive faults tap the volcano feeder conduits (Giammanco et al., 1995; 2013; 2024; Bruno et al., 2001; Caltabiano et al., 2004).

The year 2018 was actually marked by volcanic events that were interpreted as preparatory to the December 24-27 short-lived but violent flank eruption, in particular in terms of intrusion and shallow emplacement of new gas-rich magma (Aloisi et al., 2020; Borzi et al., 2020; Calvari et al., 2020). Therefore, the overall decrease in hydrothermal activity observed in the second half of 2018 at the surveyed areas would reflect the rapid upward motion of magma within the central conduit of the volcano that preceded the flank eruption.

An interesting result of our surveys was that, whatever the level of volcanic activity at Mt. Etna, both the SR and the NER hydrothermal systems are crossed by structural pathways to fluid flow that remained constantly active in driving deep fluids toward the surface (i.e. the 1776-1892 fissures in the case of SR and the 2002 fissure in the case of the NER). Other minor pathways seemed to be active only during periods of higher volcanic activity, due to fast rise of gas-rich magma and/or to significant deep accumulation of magma within the volcano. This behavior is similar to that already observed at Mt. Etna in a small steamy area fed by a hydrothermal body located on the upper southern flank of the volcano near its summit craters, where degassing faults activated according to the position and depth of magma below the surface (Maucourant et al., 2014). The conceptual models of fig. 8 show our interpretation of the data acquired both in space and in time across the SR and the NER in 2017 and 2018, as a function of the level of volcanic activity.

This model seems to be validated also by recent preliminary data from a continuous monitoring station placed inside the 2002 vent of the NER surveyed in this investigation. Those data showed interesting volcano-related temporal changes, mainly regarding the concentration of the CO_2 emitted from the fumaroles at the vent bottom (Donatucci et al., 2020; Falsaperla et al., 2020).

The variations observed in the gravity data from 2020 to 2021 could also be interpreted in terms of the transfer of new gas-rich magma from deeper to shallower levels of Mt. Etna's feeder system. In fact, these changes are

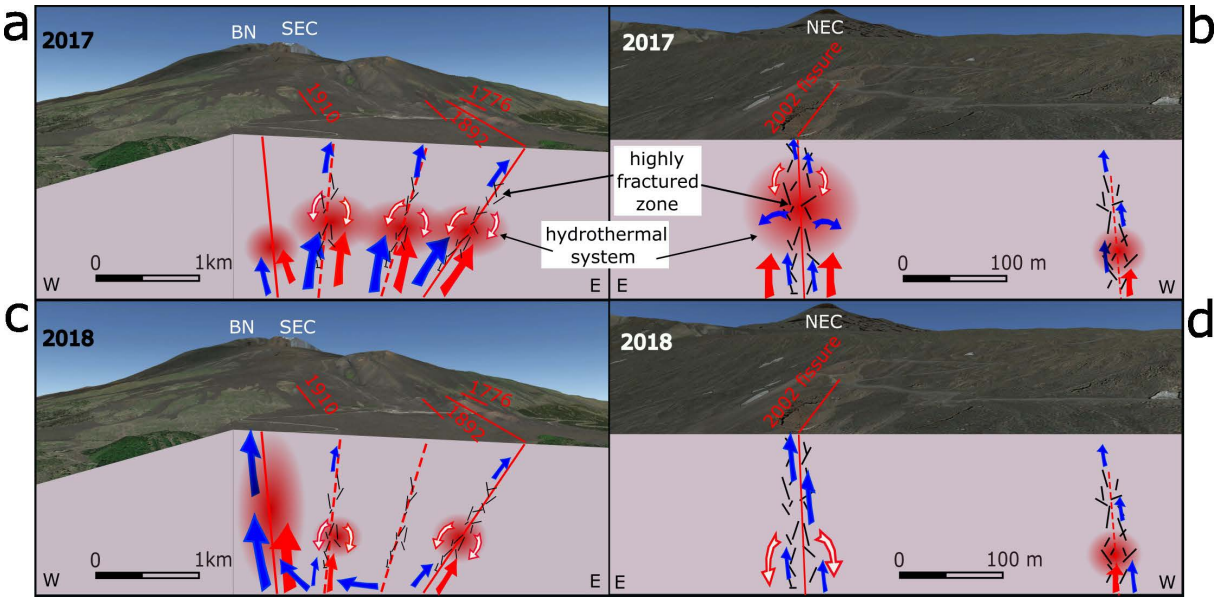

Figure 8. Schematic model of transfer and surface release of magmatic and/or hydrothermal fluids at Mt. Etna, based on the field data collected during the present investigation: (a) South Rift in 2017; (b) North East Rift in 2017; (c) South Rift in 2018; (d) North East Rift in 2018. Red arrows indicate motion of high-enthalpy fluids (the size of arrows is proportional to the intensity of fluid motion); downward-directed white arrows indicate the direction of descending condensation fluid in hydrothermal convective cells; blue arrows indicate motion of magmatic gas such as, primarily, CO_2 (the size of arrows is proportional to the intensity of fluid motion). The main eruptive fissures are shown with their date. Main faults/fissures are shown with continuous red lines; minor faults/fractures are shown with dashed red lines. BN = Bocca Nuova; SEC = SouthEast Crater; NEC = NorthEast Crater.

consistent with a greater input of low-density magmatic fluids from fresh magma degassing that likely fed the shallow hydrothermal system along the upper SR area.

6. Conclusions

Our multidisciplinary approach proved invaluable in the detection and delineation of the extent and morphology of shallow hydrothermal bodies situated along faults and other volcano-tectonic structures that traverse the volcano flanks, which was the main scope of this work. The methodologies employed are straightforward and readily applicable in the field. Several parameters such as soil CO_2 efflux, soil heat flux and SP can be processed immediately following data acquisition, enabling rapid assessment of local conditions and more precise targeting of prospecting. This study represents the first instance of extensive and repeated surveys on this volcano specifically aimed at hydrothermal system characterization, integrating a wide range of parameters across multiple Earth Sciences disciplines. Our findings confirm the presence of well-developed hydrothermal bodies in both the South Rift (SR) and the Northeast Rift (NER), functioning as persistent fluid circulation zones. These systems are initially fueled by magma degassing and subsequently enriched with hydrothermal components. The level of detail achieved allowed us to identify and spatially constrain several hydrothermal cells to depths of several hundred meters below the surface. Repeating the surveys after several months, both in terms of geochemical and of geophysical parameters, allowed us to detect changes in the spatial extent of the identified hydrothermal bodies and the intensity of energy and mass release from them. These variations were attributed to fluctuating inputs of magmatic fluids, involving both increases and decreases, likely linked to magma transfers between the lower and upper segments of Mt. Etna's feeding system preceding the 2018 flank eruption and subsequently the 2020-2021 sequence of paroxysmal eruptions at the summit craters of the volcano. Furthermore, the observed temporal variations in gravity highlight the dynamic nature of this sector of the volcano, underscoring the importance of comprehensive spatio-temporal monitoring to detect changes in volcanic activity. The regular monitoring of the investigated parameters is, therefore, essential and should be complemented by the integration of advanced technologies, such as unmanned aerial vehicles (UAVs) equipped for magnetic, thermal and CO_2 measurements, as well as continuous gravity monitoring stations. Furthermore, adding numerical simulations (e.g. thermal or fluid flow modelling) would significantly improve the quantitative interpretation of the observed phenomena. Ideally, deeper temperature measurements or borehole data would help to constrain the vertical extent of the convective systems, but unfortunately these are not currently available.

The findings of this study emphasize the importance of conducting surveys that assess gas and heat emissions, in addition to the geophysical properties of rocks, particularly their density and magnetization. This integrated approach is especially relevant for investigating hydrothermal systems located along rift zones on volcano flanks. Applying this methodology enhances the detection of magma movement and thus contributes to improved forecasting of volcanic eruptions.

Our approach can also be applied to other basaltic volcanoes where hydrothermal activity is not immediately apparent. This could lead to the identification of deep or concealed hydrothermal systems and improve our understanding of the interactions between local tectonic structures, eruptive fractures, particularly those along stable rift zones of varying scales and magma dynamics.

Data availability statement. Data can be made available by the authors upon request.

Acknowledgements. We acknowledge the Ente Parco dell'Etna for letting us work inside protected areas. We also thank A. Cinquegrani, C. Tubbiolo and K. Kuppenbender for their help during the field collection of data. This work was partly supported from CNR/DTA-INGV Agreement "Caratterizzazione di risorse geotermiche delle Regioni del Mezzogiorno d'Italia", within the project "Atlante Geotermico delle Regioni Mezzogiorno".

References

Acocella, V. and M. Neri (2003). What makes flank eruptions? The 2001 Mount Etna eruption and its possible triggering mechanisms, Bull. Volcanol., 65, 517-529, doi:10.1007/s00445-003-0280-3.

Aiuppa, A., P. Allard, W. D'Alessandro, S. Giammanco et al. (2004). Magmatic gas leakage at Mount Etna (Sicily, Italy): relationships with the volcano-tectonic structures, the hydrological pattern and the eruptive activity, Bonaccorso, A., S. Calvari, M. Coltelli, C. Del Negro et al. (Eds.), Mt. Etna: Volcano Laboratory, Am. Geophys. Union, Washington, DC, 129-145, 9781118665794, doi:10.1029/143GM09.

Alparone, S., D. Andronico, S. Giammanco and L. Lodato (2004). A multidisciplinary approach to detect active pathways for magma migration and eruption in a basaltic volcano: the upper southern flank of Mt. Etna (Sicily, Italy) before the 2001 eruption, J. Volcanol. Geoth. Res., 136, 121-140, doi:10.1016/j.jvolgeores.2004.05.014.

Aloisi, M., A. Bonaccorso, F. Cannavò, G. Currenti et al. (2020). The 24 December 2018 eruptive intrusion at Etna volcano as revealed by multidisciplinary continuous deformation networks (CGPS, borehole strainmeters and tiltmeters), J. Geophys. Res. Solid Earth, 125, e2019JB019117, doi:10.1029/2019JB019117.

Angell, R. F., T. Svejcar, J. Bates, N. Z. Saliendra et al. (2001). Bowen ratio and closed chamber carbon dioxide flux measurements over sagebrush steppe vegetation, Agr. Forest Meteorol., 108, 153-161, doi:10.1016/S0168-1923(01)00227-1.

Aubert, M. L., R. Auby, F. Bourlet and Y. Bourlet (1984). Contribution à la surveillance de l'activité de l'Etna à partir de l'étude des zones fumerolliennes, Bull. Volcanol., 47, 1039-1050, doi:10.1007/BF01952359.

Aubert, M. and J. C. Baubron (1988). Identification of a hidden thermal fissure in a volcanic terrain using a combination of hydrothermal convection indicators and soil-atmosphere analysis, J. Volcanol. Geoth. Res., 35, 217-225, doi:10.1016/0377-0273(88)90018-2.

Aubert, M. (1999). Practical evaluation of steady heat discharge from dormant active volcanoes: case study of Vulcarolo fissure (Mount Etna, Italy), J. Volcanol. Geoth. Res., 92, 413-429, doi:10.1016/S0377-0273(99)00088-8.

Baranov, V. (1957). A New Method for Interpretation of Aeromagnetic Maps, Pseudo-Gravimetric Anomalies, Geophys., 22, 359-363, doi:10.1190/1.1438369.

Baubron, J.-C. (1996). Prospection, caractérisation et variabilité temporelle d'émanations gazeuses diffuses à l'Etna (Sicile, Italie). Années 1993 et 1994. Contract EV5V-CT92-0177, Rapport BRGM R 38820 dr/hgt 96, BRGM, France, 1-74.

Behncke, B. and M. Neri (2003a). The July-August 2001 eruption of Mt. Etna (Sicily), Bull. Volcanol., 65, 461-476, doi:10.1007/s00445-003-0274-1.

Behncke, B. and M. Neri (2003b). Cycles and trends in the recent eruptive behaviour of Mount Etna (Italy), Can. J. Earth Sci., 40, 1405-1411, doi:10.1139/E03-052.

Berrino, G. (2000). Combined gravimetry in the observation of volcanic processes in Southern Italy, J. Geodyn., 30, 371-388, doi:10.1016/S0264-3707(99)00072-1.

Bonforte, A., G. Fanizza, F. Greco, A. Matera et al. (2017). Long-term dynamics across a volcanic rift: 21 years of microgravity and GPS observations on the southern flank of Mt. Etna volcano, J. Volcanol. Geotherm. Res., 344, 174-184, doi:10.1016/j.jvolgeores.2017.06.005.

Borzi, A. M., M. Giuffrida, F. Zuccarello, M. Palano et al. (2020). The Christmas 2018 eruption at Mount Etna: Enlightening how the volcano factory works through a multiparametric inspection, Geochemistry, Geophysics, Geosystems, 21, e2020GC009226. doi:10.1029/2020GC009226.

Branca, S. and P. Del Carlo (2005). Types of eruptions of Etna Volcano AD 1670-2003: Implications for short-term eruptive behavior, Bull. Volcanol., 67, 732-742, doi:10.1007/s00445-005-0412-z.

Branca, S., M. Coltelli, G. Groppelli and F. Lentini (2011). Geological map of Etna volcano, 1:50,000 scale, Ital. J. Geosci., 130, 265-291, doi:10.3301/IJG.2011.15.

Branca, S. and V. Ferrara (2013). The morphostructural setting of Mount Etna sedimentary basement (Italy): Implications for the geometry and volume of the volcano and its flank instability, Tectonophys., 586, 46-64, doi:10.1016/j.tecto.2012.11.011.

Branca, S., F. D'Ajello Caracciolo, A. B. Malaguti and F. Speranza (2019). Constraining age and volume of lava flow invasions of the Alcantara valley, Etna volcano (Italy). New insights from paleomagnetic dating and 3D magnetic modeling, J. Volcanol. Geoth. Res., 374, 13-25, doi:10.1016/j.jvolgeores.2019.02.009.

Bristow, K. L., R. D. White and G. J. Kluitenberg (1994). Comparison of single and dual probes for measuring soil thermal properties with transient heating, Australian J. Soil Res., 32, 447-464.

Bruijn, P. J., I. A. van Haneghem and J. Schenk (1983). An improved nonsteady-state probe method for measurements in granular materials. Part 1: Theory, High Temp. High Press., 15, 359-366.

Bruno, N., T. Caltabiano, S. Giammanco and R. Romano (2001). Degassing of SO_2 and CO_2 at Mount Etna (Sicily) as an indicator of pre-eruptive ascent and shallow emplacement of magma, J. Volcanol. Geoth. Res., 110, 137-153, doi:10.1016/S0377-0273(01)00201-3.

Budetta, G., M. Grimaldi and G. Luongo (1989). Variazioni di gravità nell'area etnea (1986-1989), Boll. Gruppo Nazionale per la Vulcanologia, 5, 137-146.

Budetta, G., D. Carbone and F. Greco (1999). Subsurface mass redistributions at Mount Etna (Italy) during the 1995-96 explosive activity detected by microgravity studies, Geoph. J. Int., 138, 77-88.

Caltabiano, T., M. Burton, S. Giammanco, P. Allard et al. (2004). Volcanic gas emissions from the summit craters and flanks of Mt. Etna, 1987-2000, Bonaccorso, A., S. Calvari, M. Coltelli, C. Del Negro et al. (Eds.), Mt. Etna: Volcano Laboratory, Am. Geophys. Union, Washington, DC, 111-128, 9781118665794, doi:10.1029/143GM08.

Calvari, S., G. Bilotta, A. Bonaccorso, T. Caltabiano et al. (2020). The VEI 2 Christmas 2018 Etna eruption: a small but intense eruptive event or the starting phase of a larger one?, Remote Sens., 12, 905, doi:10.3390/rs12060905.

Cannata, A., G. Giudice, S. Gurrieri, P. Montalto et al. (2009). Relationship between soil CO_2 flux and volcanic tremor at Mt. Etna: Implications for magma dynamics, Environ. Earth Sci., 61, 477-489, doi:10.1007/s12665-009-0359-z.

Carapezza, M. L., T. Ricci, M. Ranaldi and L. Tarchini (2009). Active degassing structures of Stromboli and variation in diffuse CO_2 output related to the volcanic activity, J. Volcanol. Geoth. Res., 182, 231-245, doi:10.1016/j.jvolgeores.2008.08.006.

Carbone, D., G. Budetta and F. Greco (2003). Possible mechanisms of magma redistribution under Mt Etna during the 1994-1999 period detected through microgravity measurements, Geoph. J. Int., 152, 1-14, doi:10.1046/j.1365-246X.2003.01901.x.

Carbone, D. and F. Greco (2007). Review of microgravity observations at Mt. Etna: A powerful tool to monitor and study active volcanoes, Pure Appl. Geophys., 164, 769-790, doi:10.1007/s00024-007-0194-7.

Carbone, D., S. D'Amico, C. Musumeci and F. Greco (2009). Comparison between the 1994-2006 seismic and gravity data from Mt. Etna: New insight into the long-term behavior of a complex volcano, Earth Planet. Sci. Lett., 279, 282-292, doi:10.1016/j.epsl.2009.01.007.

Carbone, D., M. Aloisi, S. Vinciguerra and G. Puglisi (2014). Stress, strain and mass changes at Mt. Etna during the period between the 1991-93 and 2001 flank eruptions, Earth-Sci. Rev., 138, 454-468, doi:10.1016/j.earscirev.2014.07.004.

Chester, D. K., A. M. Duncan, J. E. Guest and C. R. J. Kilburn (1985). Mount Etna: the Anatomy of a Volcano, Chapman and Hall, London, 1-300, 978-0-412-23890-1, doi:10.1007/978-94-009-4079-6.

Chiodini, G., R. Cioni, M. Guidi, B. Raco, et al. (1998). Soil CO_2 flux measurements in volcanic and geothermal areas, Appl. Geochem., 13, 135-148, doi:10.1016/S0883-2927(97)00076-0.

Cueva, A., T. H. M. Volkman, J. van Haren, P. A. Troch et al. (2019). Reconciling Negative Soil CO_2 Fluxes: Insights from a Large-Scale Experimental Hillslope, Soil Syst., 3, 10, doi:10.3390/soilsystems3010010.

Del Negro, C. and R. Napoli (2002). Ground and marine magnetic surveys of the lower eastern flank of Etna volcano (Italy), J. Volcanol. Geotherm. Res., 114, 357-372, doi:10.1016/S0377-0273(01)00295-5.

Del Negro, C., G. Currenti, G. Solaro, F. Greco et al. (2013). Capturing the fingerprint of Etna volcano activity in gravity and satellite radar data, Sci. Rep., 3, 3089, doi:10.1038/srep03089.

Diliberto, I. S., E. Gagliano Candela, S. Morici, G. Pecoraino et al. (2018). Changes in heat released by hydrothermal circulation monitored during an eruptive cycle at Mt. Etna (Italy), Bull. Volcanol., 80, 31, doi:10.1007/s00445-018-1198-0.

Di Maio, R. and G. Berrino (2016). Joint analysis of electric and gravimetric data for volcano monitoring. Application to data acquired at Vulcano Island (southern Italy) from 1993 to 1996, J. Volcanol. Geotherm. Res., 327, 459-468, doi:10.1016/j.jvolgeores.2016.09.013.

Donatucci, A., F. Sortino, S. Giammanco, B. Behncke et al. (2020). Geochemical study of high temperature fumaroles and non-plume degassing in Mt Etna's summit area, in Proceedings 4th Rittmann Conference, Catania, Italy, Miscellanea INGV, 52, 203, ISSN: 2039-6651.

Falsaperla, S., T. Caltabiano, A. Donatucci, S. Giammanco et al. (2020). Integrated monitoring of soil gases, plume SO_2 and volcanic tremor to detect impulsive magma transfer at Mt. Etna volcano (Italy), in Proceedings EGU General Assembly 2020, Vienna, Austria, EGU2020-14698, doi:10.5194/egusphere-egu2020-14698.

Farrar, C. D., M. L. Sorey, W. C. Evans, J. F. Howle et al. (1995). Forest-killing diffuse CO_2 emission at Mammoth Mountain as a sign of magmatic unrest, Nature, 376, 675-678, doi:10.1038/376675a0.

Federico, C., O. Cocina, S. Gambino, A. Paonita et al. (2023). Inferences on the 2021 Ongoing Volcanic Unrest at Vulcano Island (Italy) through a Comprehensive Multidisciplinary Surveillance Network, Remote Sens., 15, 1405, doi:10.3390/rs15051405.

Ferrara, V. and G. Pappalardo (2008). The hydrogeological map of the Etna volcanic massif as useful tool for groundwater resources management, It. J. Eng. Geol. Environ, 1, 77-89, doi:10.4408/IJEGE.2008-01.S-06.

Finizola, A., F. Sortino, J. F. Lénat and M. Valenza (2002). Fluid circulation at Stromboli volcano (Aeolian Island, Italy), from self-potential and CO_2 surveys, J. Volcanol. Geoth. Res., 116, 1-18, doi:10.1016/S0377-0273(01)00327-4.

Finizola, A., J. F. Lénat, O. Macedo, D. Ramos et al. (2004). Fluid circulation and structural discontinuities inside Misti Volcano (Peru) inferred from self-potential measurements, J. Volcanol. Geoth. Res., 135, 343-360, doi:10.1016/j.jvolgeores.2004.03.009.

Frank, A. B., M. A. Liebig and J. D. Hanson (2002). Soil carbon dioxide fluxes in northern semiarid grasslands, Soil Biol. Biochem., 34, 1235-1241, doi:10.1016/S0038-0717(02)00062-7.

Garduño, V. H., M. Neri, G. Pasquarè, A. Borgia et al. (1997). Geology of NE rift of Mount Etna, Sicily (Italy), Acta Vulcanol., 9, 91-100.

Gemmellaro, C. (1858). La vulcanologia dell'Etna, Tipografia Accademia Gioenia, Catania, 1-267.

Giammanco, S. and P. Bonfanti (2009). Cluster analysis of soil CO_2 data from Mt. Etna (Italy) reveals volcanic influences on temporal and spatial patterns of degassing, Bull. Volcanol., 71, 201-218, doi:10.1007/s00445-008-0218-x.

Giammanco, S., S. Gurrieri and M. Valenza (1995). Soil CO_2 degassing on Mt. Etna (Sicily) during the period 1989-1993: discrimination between climatic and volcanic influences, Bull. Volcanol., 57, 52-60, doi:10.1007/BF00298707.

Giammanco, S., S. Inguaggiato and M. Valenza (1998). Soil and fumarole gases of Mount Etna: Geochemistry and relations with volcanic activity, J. Volcanol. Geoth. Res., 81, 297-310, doi:10.1016/S0377-0273(98)00012-2.

Giammanco, S., S. Gurrieri and M. Valenza (1999). Geochemical investigations applied to active fault detection in a volcanic area: the North-East Rift on Mt. Etna (Sicily, Italy), Geoph. Res. Lett., 26, 2005-2008, doi:10.1029/1999GL900396.

Giammanco, S. and G. Pecoraino (2002). Temporal variations of soil and fumarole gases at Mt. Etna volcano (Italy) during 2000-2001, Proceedings 6th International Symposium on Geochemistry of Earth's Surface, Honolulu, Hawaii, USA, 319-323.

Giammanco, S., F. Parello, B. Gambardella, R. Schifano et al. (2007). Focused and diffuse effluxes of CO_2 from mud volcanoes and mofettes south of Mt. Etna (Italy), J. Volcanol. Geotherm. Res., 165, 46-63, doi:10.1016/j.jvolgeores.2007.04.010.

Giammanco, S., M. Neri, G. G. Salerno, T. Caltabiano et al. (2013). Evidence for a recent change in the shallow plumbing system of Mt. Etna (Italy): gas geochemistry and structural data during 2001-2005, J. Volcanol. Geotherm. Res., 251, 90-97, doi:10.1016/j.jvolgeores.2012.06.001.

Giammanco, S., G. Salerno, A. La Spina, P. Bonfanti et al. (2024). Tracing Magma Migration at Mt. Etna Volcano during 2006-2020, Coupling Remote Sensing of Crater Gas Emissions and Ground Measurement of Soil Gases, Remote Sens., 16, 1122, doi:10.3390/rs16071122.

Gillot, P. Y., G. Kie¡er and R. Romano (1994). The evolution of Mount Etna in the light of potassium-argon dating, Acta Vulcanol., 5, 81-87.

Grauch, V. J. S., M. R. Hudson and S. A. Minor (2001). Aeromagnetic expression of faults that offset basin fill, Albuquerque basin, New Mexico, Geophys., 66, 707-720, doi:10.1190/1.1444961.

Gottsmann, J., H. Rymer and L. Wooller (2005). On the interpretation of gravity variations in the presence of active hydrothermal systems: insights from the Nisyros caldera, Greece, Geophys. Res. Lett., 32, L23310, doi:10.1029/2005GL024061.

Gottsmann, J., A. Folch and H. Rymer (2006). Unrest at Campi Flegrei: A contribution to the magmatic versus hydrothermal debate from inverse and finite element modeling, J. Geophys. Res., 111, B07203, doi:10.1029/2005JB003745.

Gottsmann, J., R. Carniel, N. Coppo, L. Wooller et al. (2007). Oscillations in hydrothermal systems as a source of periodic unrest at caldera volcanoes: Multiparameter insights from Nisyros, Greece, Geophys. Res. Lett., 34, L07307, doi:10.1029/2007GL029594.

Granieri, D., G. Chiodini, W. Marzocchi and R. Avino (2003). Continuous monitoring of CO_2 soil diffuse degassing at Phlegraean Fields (Italy): Influence of environmental and volcanic parameters, Earth Planet. Sci. Lett., 212, 167-179, doi:10.1016/S0012-821X(03)00232-2.

Greco, F., G. Currenti, C. Del Negro, R. Napoli et al. (2010). Spatiotemporal gravity variations to look deep into the southern flank of Etna volcano, J. Geophys. Res., 115, B11411, doi:10.1029/2009JB006835.

Greco, F., G. Currenti, G. D'Agostino, A. Germak et al. (2012). Combining relative and absolute gravity measurements to enhance volcano monitoring at Mt Etna (Italy), Bull. Volcanol., 74, 1745-1756, doi:10.1007/s00445-012-0630-0.

Greco, F., G. Currenti, M. Palano, A. Pepe et al. (2016). Evidence of a shallow persistent magmatic reservoir from joint inversion of gravity and ground deformation data: The 25-26 October 2013 Etna lava fountaining event, Geophys. Res. Lett., 43, 3246-3253, doi:10.1002/2016GL068426.

Greco, F., A. Bonforte and D. Carbone (2022). A long-term charge/discharge cycle at Mt. Etna volcano revealed through absolute gravity and GPS measurements, J. Geodesy, 96, 101, doi:10.1007/s00190-022-01692-z.

Grobbe, N. and S. Barde-Cabusson (2019). Self-Potential studies in volcanic environments: a cheap and efficient method for multiscale fluid-flow investigations. Int. J. Geophys., 2019, 985824, doi:10.1155/2019/2985824.

Harris, A. J. L., L. Flynn, D. A. Rothery, C. Oppenheimer et al. (1999). Mass flux measurements at active lava lakes: Implications for magma recycling, J. Geophys. Res., 104, 7117-7136, doi:10.1029/98JB02731.

Hashimoto, T. and Y. Tanaka (1995). A large self-potential anomaly at Unzen volcano, Shimabara Peninsula Kyushu Island, Japan, Geophys. Res. Lett., 22, 191-194, doi:10.1029/94GL03077.

Hernández, P. A., K. Notsu, J. M. Salazar, T. Mori et al. (2001). Carbon Dioxide Degassing by Advective Flow from Usu Volcano, Japan, Science, 292, 5514, 83-86, doi:10.1126/science.1058450.

Jackson, D. B. and J. Kauahikaua (1987). Regional self-potential anomalies at Kilauea Volcano, In: Volcanism in Hawaii, R. W. Decker, T. L. Weight, P. H. Stauffer, (Editors), U.S. Geological Survey Prof. Paper, 1350, 2, Washington, 947-959.

Johnston, M. J. S., J. D. Byerlee and D. Lockner (2001). Rapid fluid disruption: a source for selfpotential anomalies on volcanoes, J. Geophys. Res., 106, B3, 4327-4335, doi:10.1029/2000JB900349.

Kieffer, G. (1975). Sur l'existence d'une "Rift zone" à l'Etna (Sicile), C.R. Acad. Sci., Paris, D 280, 236-266.

Kieffer, G. (1983). L'évolution structurale de l'Etna (Sicile) et les modalités du controle tectonique et volcanotectonique de son activité. Faits et hypothéses aprés les éruptions de 1978 et 1979, Rev. Géol. Dynam. Géograph. Phys., 24, 2, 129-152.

La Scala, N., J. Marques, G. T. Pereira and J. E. Cora (2000). Short-term temporal changes in the spatial variability model of CO_2 emissions from a Brazilian bare soil, Soil Biol. Biochem., 32, 1459-1462, doi:10.1016/S0038-0717(00)00051-1.

Lénat, J. F. (2007). Retrieving self-potential anomalies in a complex volcanic environment: an SP/elevation gradient approach. Near Surf. Geophys., 5, 161-172, doi:10.3997/1873-0604.2006028.

Lo Giudice, E., G. Patanè, R. Rasà and R. Romano (1982). The structural framework of Mt. Etna, Mem. Soc. Geol. Ital., 23, 125-158.

Lowrie, W. and D. V. Kent (2004). Geomagnetic polarity timescales and reversal frequency regimes, in: Timescales of the Palaeomagnetic Field, J. E. T. Channell, D. V. Kent, W. Lowrie and J. Meert (Editors.), American Geophysical Union, Washington DC, 117-129, doi:10.1029/145GM09.

Ma, J., Y. Li and R. Liu (2015). The abiotic contribution to total CO_2 flux for soils in arid zone, Biogeosciences Discuss., 12, 11217-11244, doi:10.5194/bgd-12-11217-2015.

Maestre, F. T. and J. Cortina (2003). Small-scale spatial variation in soil CO_2 efflux in a Mediterranean semiarid steppe, Appl. Soil Ecol., 23, 199-209, doi:10.1016/S0929-1393(03)00050-7.

Massenet, F. and P. Van Ngoc (1985). Mapping and surveillance of active fissure zones on a volcano by the self-potential method, Etna, Sicily, J. Volcanol. Geotherm. Res., 24, 315-338, doi:10.1016/0377-0273(85)90075-7.

Maucourant, S., S. Giammanco, F. Greco, S. Dorizon et al. (2014). Geophysical and geochemical methods applied to investigate fissure-related hydrothermal systems on the summit area of Mt. Etna volcano (Italy), J. Volcanol. Geotherm. Res., 280, 111-125, doi:10.1016/j.jvolgeores.2014.05.014.

Mielnick, P. C. and W. A. Dugas (2000). Soil CO_2 flux in a tallgrass prairie, Soil Biol. Biochem., 32, 221-228, doi:10.1016/S0038-0717(99)00150-9.

Mouginis-Mark, P. J., J. A. Crisp and J. H. Fink (2000). Remote Sensing of Active Volcanism, Geophysical Monograph Series, Vol. 116, American Geophysical Union, Washington DC, 1-272, ISBN: 978-1-118-66451-3.

Napoli, R., G. Currenti, C. Del Negro, F. Greco et al. (2008). Volcanomagnetic evidence of the magmatic intrusion on 13th May 2008 Etna eruption, Geophys. Res. Lett., 35, L22301, doi:10.1029/2008GL035350.

Napoli, R., G. Currenti, S. Giammanco, F. Greco et al. (2020). Imaging the Salinelle Mud Volcanoes (Sicily, Italy) using integrated geophysical and geochemical surveys, Ann. Geophys., 63, 4, PE442, doi:10.4401/ag-8215.

Napoli, R., G. Currenti and A. Sicali (2021). Magnetic signatures of subsurface faults on the northern upper flank of Mt. Etna (Italy), Ann. Geophys., 64, 1, PE108, doi:10.4401/ag-8582.

Neri, M., V. Acocella, B. Behncke, S. Giammanco et al. (2011). Structural analysis of the eruptive fissures at Mount Etna (Italy), Ann. Geophys., 54, 5, 2011, doi:10.4401/ag-5332.

Nicolosi, I., F. D'Ajello Caracciolo, S. Branca, G. et al. (2014). Volcanic conduit migration over a basement landslide at Mount Etna (Italy), Sci. Rep., 4, 5293, doi:10.1038/srep05293.

Obrist, D., E. H. Delucia and J. A. Arnone III (2003). Consequences of wildfire on ecosystems CO_2 and water vapour fluxes in the Great Basin, Glob. Change Biol., 9, 563-574, doi:10.1046/j.1365-2486.2003.00600.x.

Oppenheimer, C. and P. Francis (1997). Remote sensing of heat, lava and fumarole emissions from Erta 'Ale volcano, Ethiopia, Int. J. Remote Sens., 18, 8, 1661-1692, doi:10.1080/014311697218043.

Pecoraino, G. and S. Giammanco (2005). Geochemical Characterization and Temporal Changes in Parietal Gas Emissions at Mt. Etna (Italy) During the Period July 2000-July 2003, Terr., Atmosph. Ocean. Sci., 16, 4, 805-841, doi:10.3319/TAO.2005.16.4.805(GIG).

Pérez, N. M., P. A. Hernádez, E. Padrón, R. Cartagena et al. (2006). Anomalous Diffuse CO_2 Emission prior to the January 2002 Short-term Unrest at San Miguel Volcano, El Salvador, Central America, Pure Appl. Geophys., 163, 883-896, doi:10.1007/s00024-006-0050-1.

Pham Van Ngoc, F. Massenet and W. Tjetjep (1981). Campagne géophysique à l'Etna mai-juin 1981. Bull. PIRPSEV 47, CNRS, Paris.

Ponte, G. (1927). Il Vulcarolo sull'Etna e la utilizzazione del suo vapore acqueo, Boll. Acc. Gioenia Sc. Nat., 57, 1-2, 14-17.

Raich, J. W. and W. H. Schlesinger (1992). The global carbon dioxide flux in soil respiration and its relationship to vegetation and climate, Tellus, 44B, 81-99, doi:10.1034/j.1600-0889.1992.t01-1-00001.x.

Raich, J. W. and A. Tufekcioglu (2000). Vegetation and soil respiration: Correlations and controls, Biogeochem., 48, 71-90, doi:10.1023/A:1006112000616.

Reth, S., M. Gockede and E. Falge (2005). CO_2 efflux from agricultural soils in Eastern Germany – comparison of a closed chamber system with eddy covariance measurements, Theor. Appl. Climatol., 80, 105-120, doi:10.1007/s00704-004-0094-z.

Revil, A., H. Schwager, L. M. Cathles and P. D. Manhardt (1999). Streaming potential in porous media 2. Theory and application to geothermal systems, J. Geophys. Res., 104, B9, 20033-20048, doi:10.1029/1999JB900090.

Revil, A. and A. Jardani (2013). The Self-Potential method: theory and applications in environmental geosciences, Cambridge University Press, Cambridge, 1-369, ISBN:9781139094252, doi:10.1017/CBO9781139094252.

Rogie, J. D., D. M. Kerrick, M. L. Sorey, G. Chiodini et al. (2001). Dynamics of carbon dioxide emission at Mammoth Mountain, California, Earth Planet. Sci. Lett., 188, 535-541, doi:10.1016/S0012-821X(01)00344-2.

Rittmann, A. (1973). Structure and evolution of Mount Etna, Phil. Trans. R. Soc. Lond., A 274, 5-16.

Sinclair, A. J. (1974). Selection of thresholds in geochemical data using probability graphs, J. Geochem. Explor., 3, 129-149, doi:10.1016/0375-6742(74)90030-2.

Spampinato, L., S. Calvari, C. Oppenheimer and E. Boschi (2011). Volcano surveillance using infrared cameras, Earth Sci. Rev., 106, 63-91, doi:10.1016/j.earscirev.2011.01.003.

Tanguy, J.-C., M. Condomines and G. Kieffer (1997). Evolution of the Mount Etna magma: Constraints on the present feeding system and eruptive mechanism, J. Volcanol. Geotherm. Res., 75, 3-4, 221-250, doi:10.1016/S0377-0273(96)00065-0.

Todesco, M. and G. Berrino (2005). Modeling hydrothermal fluid circulation and gravity signals at the Phlegraean Fields caldera, Earth Planet. Sci. Lett., 240, 328-338, doi:10.1016/j.epsl.2005.09.016.

Tikku, A. A., D. C. McAdoo, M. S. Schenewerk and E. C. Willoughby (2006). Temporal fluctuations of microseismic noise in Yellowstone's Upper Geyser Basin from a continuous gravity observation, Geophys. Res. Lett., 33, L11306, doi:10.1029/2006GL026113.

Tric, E., J. P. Valet, P. Y. Gillot and I. Lemeur (1994). Absolute paleointensities between 60 and 160 kyear BP from Mount Etna (Sicily), Phys. Earth Planet. Inter., 85, 113-129, doi:10.1016/0031-9201(94)90011-6.

van Haneghem, I. A., J. Schenk and H. P. A. Boshoven (1983). An improved nonsteady-state probe method for measurements in granular materials. Part II: Experimental results, High Temp. High Press., 15, 367-374.

van Loon, W. K. P., I. A. van Haneghem and J. Schenk (1989). A new model for the non-steady-state probe method to measure thermal properties of porous media, Int. J. Heat Mass Transfer, 32, 8, 1473-1481, doi:10.1016/0017-9310(89)90069-0.

Villasante-Marcos, V., A. Finizola, R. Abella, S. Barde-Cabusson et al. (2014). Hydrothermal system of Central Tenerife Volcanic Complex, Canary Islands (Spain), inferred from self-potential measurements, J. Volcanol. Geoth. Res., 272, 59-77, doi:10.1016/j.jvolgeores.2013.12.007.

Viveiros, F., T. Ferreira, J. Cabral Vieira, C. Silva et al. (2008). Environmental influences on soil CO_2 degassing at Furnas and Fogo volcanoes (São Miguel Island, Azores archipelago), J. Volcanol. Geotherm. Res., 177, 883-893, doi:10.1016/j.jvolgeores.2008.07.005.

Wang, W. F., X. Chen, Z. Pu, X. L. Yuan et al. (2015). Negative Soil Respiration Fluxes in Unneglectable Arid Regions, Pol. J. Environ. Stud., 24, 905-908, doi:10.15244/pjoes/23878.

Zlotnicki, J., G. Boudon, J. P. Viodé, J. F. Delarue et al. (1998). Hydrothermal circulation beneath Mount Pelee inferred by self-potential surveying. Structural and tectonic implications, J. Volcanol. Geotherm. Res., 84, 73-9, doi:10.1016/S0377-0273(98)00030-4.

***CORRESPONDING AUTHOR: Salvatore GIAMMANCO**,
Istituto Nazionale di Geofisica e Vulcanologia, Osservatorio Etneo-Sezione di Catania, Catania, Italy
e-mail: salvatore.giammanco@ingv.it